FAST: A Future Aircraft Sizing Tool for Conventional and Electrified Aircraft Design

Paul R. Mokotoff*, Maxfield Arnson*, Yi-Chih Wang*, and Gokcin Cinar†
University of Michigan, Ann Arbor, Michigan 48109

Electrified aircraft are a promising solution to reduce aviation's carbon footprint across general and commercial aviation sectors. However, existing computational tools for aircraft design require information about the aircraft's configuration, forcing the designer to down-select before optimizing their design. As a result of the limited flexibility, sub-optimal system architectures may be selected during the early phases of conceptual design. To address this, the Future Aircraft Sizing Tool (FAST), an open-source, MATLAB-based tool, was developed as a propulsion system-agnostic tool for early-phase conceptual design. Using limited design parameters, FAST facilitates rapid and comprehensive aircraft sizing and performance evaluation, utilizing an extensive database of over 450 historical aircraft. Both data-driven and physics-based models are combined to seamlessly integrate new electrification technologies into a design while rapidly predicting its performance. This capability enables early-stage design space exploration to rigorously assess a wide range of propulsion architectures, energy sources, and operational strategies for novel aircraft configurations. This paper presents the key features of FAST, including workflows for aircraft sizing and analysis. The paper also presents a case study involving a commercial freighter, demonstrating FAST's ability to perform design space exploration and early-phase trade studies.

I. Introduction

Over the last decade, electrified aircraft design has gained significant attention as a promising technology to curb aviation's harmful CO_2 emission contributions. Electrified aircraft, encompassing fully electric, hybrid-electric, and turboelectric configurations, integrate components such as electric motors, generators, power converters, and batteries into the powertrain. The primary system-level benefits associated with aircraft electrification include reduced CO_2 emissions during operation due to decreased fuel burn, as well as reduced thermal and acoustic signatures. These benefits come from decoupling the gas turbine engine and propulsor, allowing them to operate at their own optimal speeds [1]. Significant funding and efforts have been invested into electrified aircraft design, particularly within the

This paper was previously presented as a conference paper at the AIAA SciTech Forum, held January 12-16, 2025 in Orlando, FL. The AIAA paper number was 2025-2374.

*Graduate Research Assistant, Department of Aerospace Engineering, AIAA Student Member.
†Assistant Professor, Department of Aerospace Engineering, AIAA Senior Member; Corresponding Author (cinar@umich.edu)

Electrified Aircraft Propulsion (EAP) program at NASA [2] and their Electrified Powertrain Flight Demonstration (EPFD) Project [3]. These programs test new electrified aircraft propulsion technologies and assess the difficulties associated with integrating them into future aircraft concepts [3]. These programs have yielded many novel conceptual aircraft designs, such as NASA's Subsonic Single Aft Engine (SUSAN) [4] and Single-Aisle Turboelectric Aircraft with Aft Boundary Layer Propulsion (STARC-ABL) [5] concepts.

Designing electrified aircraft requires comprehensive tools capable of evaluating novel propulsion architectures and their impact on the overall design. Computational design tools play a pivotal role in this process, enabling engineers to explore diverse configurations and operational strategies efficiently. However, the effectiveness of these tools often depends on their assumptions and capabilities, which may limit their applicability during the early stages of conceptual design when critical decisions about the configuration and its propulsion system are still being made. Previously developed aircraft sizing codes are reviewed to assess each one's strengths and identify areas that FAST provides new capabilities and extends existing ones.

A. Review of Current Computational Tools for Electrified Aircraft Design

Six computational tools have been developed to design advanced aircraft concepts and explore the vast design space of electrified propulsion systems. Table 1 summarizes their core capabilities and limitations.

Table 1 Features and capabilities of current aircraft design tools.

	SUAVE	LUCAS	Aviary	FAST-OAD	JPAD Modeller	E-PASS
Open-Source	✓	✗	✓	✓	✗	✗
Requires Component/ Subsystem Definitions	✓	✓	✓	✓	✓	✓
Interface with Optimization Tools	✓	✓	✓	✓	✓	✓
Evaluate any Propulsion System	✓	✗	✗	✗	✗	✓
Rapid (< 1-minute) Low-Fidelity Analysis	✗	✗	✗	✓	✓	✗

One of the long standing aircraft design tools available is SUAVE [6], an open-source, Python-based code developed at Stanford University that analyzes (un)conventional concepts using multi-fidelity physics-based models. These unconventional concepts are easily analyzed by SUAVE's energy networks, allowing any propulsion system architecture

to be modeled. Additionally, SUAVE includes weight build-ups for tube-and-wing, blended wing body, unmanned aerial, and electric vertical takeoff and landing vehicles. One of SUAVE's distinguishing features is that it is built to be wrapped by optimizers for aircraft design using multidisciplinary design optimization. This is ideal for late conceptual design and early preliminary design once the aircraft configuration is down-selected and design refinement is underway. However, SUAVE's lowest-fidelity aerodynamic analysis employs a vortex lattice method, which can be too computationally demanding and prohibit rapid design space exploration. For early design studies, a drag polar model involving empirical relations is more desirable for its superior computational efficiency and simplicity.

Another aircraft design tool built upon SUAVE is LUCAS [7], which integrates a unified propulsion system model, boundary layer ingestion technology models, and advanced aerodynamic analysis models into the analysis. LUCAS wraps pyOptSparse [8] – an optimization framework that interfaces between any gradient-based or gradient-free optimization problems – around SUAVE. The wrapper allows LUCAS to easily run different aircraft-level optimizations, especially advanced aircraft concepts that include boundary layer ingestion or electrified propulsion systems. One feature that distinguishes LUCAS from other software is its unified propulsion system model, which can easily represent conventional, electrified, hybrid-electric, and fully-electric propulsion systems. This unified model relies on two electrification factors, namely the "source electrification factor", which splits the power between kerosene fuel and batteries, and the "load electrification factor", which splits the propulsive power between any gas turbine engines or electric motors [7]. However, the model only is valid for the previously mentioned propulsion architectures and cannot easily integrate other energy sources, such as hydrogen, into its model. Additionally, LUCAS is not open-source and cannot be accessed by the public.

NASA recently released Aviary [9], an open-source aircraft design program which unifies two legacy codes (FLOPS and GASP) under one software. Aviary is built upon OpenMDAO [10], an open-source framework built for tightly coupled multidisciplinary analysis and efficient derivative computation. Aviary is fully differentiated (derivatives from the analysis are computed analytically and available for use in an optimization framework), distinguishing itself from other codes. Its modular framework allows users to swap in their own analyses, particularly to replace Aviary's empirical relations for higher-fidelity physics-based models. Also, depending on the design phase, the user may select an energy-based mission analysis or a more detailed dynamics model, which models the aircraft as a point mass or two degree-of-freedom system, respectively. One limitation of Aviary, however, is that its propulsion system models are governed by a maximum two control parameters. While this allows the user to control propulsion system components independently of each other, it only permits two degrees of freedom in the propulsion architecture, thus limiting those that can be analyzed.

Another recently developed aircraft sizing tool is FAST-OAD (Fixed-wing Aircraft Sizing Tool - Overall Aircraft Design) [11], an open-source, Python-based software developed by ONERA and ISAE-SUPAERO. Like Aviary, FAST-OAD is built upon OpenMDAO, which promotes modularity and provides the ability to integrate with an MDAO

environment for more detailed aircraft design. FAST-OAD features two different mission analysis options, allowing the user to tradeoff between computational accuracy and efficiency. The default mission analysis assumes the aircraft is a point mass, using a time-step integration for all of its mission segments. However, a Breguet Range Equation-based analysis is also available. Despite the Breguet Range Equation's usefulness for rapid aircraft analyses in early-phase conceptual design, it is only applicable for conventional aircraft. If an electrified aircraft design is selected, the Breguet Range Equation is no longer valid and other approximations are needed [12, 13]. This limits the number of advanced configurations that FAST-OAD can evaluate, though there are plans to include an electric propulsion discipline in future work.

Beyond Python-based tools, JPAD Modeller [14, 15] is a Java-based aircraft design tool that harnesses semi-empirical methods and statistical regressions to size an aircraft concept. JPAD Modeller has now been commercialized [16] and is not available as an open-source tool. One unique feature included is the capability to export a CAD model of the sized aircraft, making it useful for later design phases when further analyses or manufacturing are being considered. Additionally, Genetic Algorithm and Particle Swarm optimization algorithms are built into JPAD Modeller. However, these can be computationally expensive to run because they require thousands of function evaluations and do not rely on gradient-based techniques, making them converge more slowly [17].

The Electrified Propulsion Aircraft Sizing and Synthesis (E-PASS) tool is among the first conceptual aircraft design tools designed specifically for the sizing and system-level analysis of both conventional and electrified aircraft with a variety of propulsion architectures [18–20]. Its analysis modules include component-based weight estimations, propulsion performance, aerodynamics modeling using a drag polar, an energy-based mission analysis, and physics-based electrical component models (batteries, electric motors and generators, power converters, and transmission systems). One distinguishing factor in E-PASS is its matrix-based propulsion system framework, which utilizes Graph Theory to conveniently represent propulsion system architectures and operation using matrices. The other distinguishing factor is its propulsion system-agnostic mission analysis, which leverages the matrix-based propulsion system framework to use multiple energy sources during the mission. For example, an aircraft can fly with both a gas turbine engine powered by kerosene fuel and an electric motor powered by a battery simultaneously. This capability extends beyond legacy codes like FLOPS, which only permits one energy source to be used at any given time. However, E-PASS is primarily suited for late-phase conceptual design or preliminary design stages when a baseline configuration has been established. Its higher granularity and model fidelity make it less applicable for early-phase conceptual design, where flexibility and broad design space exploration are typically prioritized.

After reviewing the tools, some significant limitations were identified. First, the tools require the aircraft's geometry to be known prior to running the analysis. This implies that design decisions have already been made about the configuration. During early-phase conceptual design, multiple configurations are being explored and the geometry may not be fully known, thus limiting the effectiveness of component-based weight estimations and geometry-based

aerodynamics analyses. A tool that can analyze an aircraft configuration without knowing the geometry is critical for early-phase conceptual design. Second, very few tools accommodate a plethora of novel propulsion system designs. Some propulsion system modeling frameworks described previously have not been generalized to accommodate energy sources beyond kerosene fuel and batteries. A general propulsion system framework is essential for permitting the designer to explore all configurations and energy source alternatives. Lastly, existing aircraft design tools that interface with high-fidelity MDAO codes are not suitable for making initial design decisions on clean-sheet aircraft designs. Using detailed analysis and optimization modules during early-phase conceptual design prevents the designer from quickly identifying the most critical design parameters that will impact the final design and require significant computational resources. However, lower-fidelity analysis modules may be suitable for wrapping within an optimizer during conceptual design. With many novel aircraft configurations and propulsion architectures being developed, there is a need for a conceptual aircraft design and analysis tool that can rapidly generate aircraft designs and allow for early-phase design space exploration while exploring different operational strategies for electrified aircraft concepts. Such a tool allows aircraft designers to explore a myriad of aircraft concepts before down-selecting on a configuration and optimizing its operational strategies.

B. Objectives: A Flexible Computational Tool for Early-Stage Aircraft Design

Based on the literature review and the NASA program office funding this work, a conceptual aircraft sizing tool must be developed to allow for rapid early-phase conceptual design, projecting existing technologies into the future, and facilitating design space exploration studies. One of NASA's primary research goals is to advance aerospace technologies and revolutionize the energy efficiency and environmental compatibility of fixed-wing transport aircraft. These transport aircraft may be smaller turboprops carrying fewer than 19 passengers (Federal Aviation Administration [FAA] Part 23 aircraft), or larger turboprops and turbofan aircraft carrying between 20 and 300 or more passengers (FAA Part 25 aircraft). Designing such aircraft requires system-level analyses to assess the interdependencies between technologies, as well as possible benefits and drawbacks. Additionally, the tool should facilitate high-level optimization for a given set of parametric mission requirements as well as aircraft- and component-level performance parameters.

With the support of NASA's EPFD and hybrid-electric research teams, the **F**uture **A**ircraft **S**izing **T**ool, **FAST**[*], was developed as an open-source, MATLAB-based aircraft sizing tool to fill this void and serve as an early-phase conceptual design tool to size an aircraft with *any* propulsion architecture. The key distinguishing features within FAST are:

1) A rapid aircraft sizing environment to facilitate design space exploration and sensitivity studies for conventional and electrified aircraft (with the ability to add other component-level models for concepts involving hydrogen or other novel fuels), with designs usually converging in less than one-minute
2) The FAST Aerobase [21], a database of over 450 conventional, kerosene-powered aircraft to drive regressions for

[*]https://dx.doi.org/10.7302/26047

predicting unknown aircraft performance parameters and propulsion system sizing estimates [22]

3) An energy-based mission analysis, which requires no assumptions about the aircraft's propulsion architecture, thus opening the possibility to compare aircraft concepts with different configurations (tube-and-wing, blended wing body, etc.) and propulsion architectures at a conceptual design-level
4) Simplified turbofan and turboprop models combined with historical data regressions for accurate engine performance analysis and fuel burn estimates
5) A visualization toolbox to render drawings of an aircraft concept both inside and outside the aircraft analysis [23]

FAST was initially implemented in MATLAB to satisfy the requirements of the NASA program office funding this work and to ensure seamless integration with existing MATLAB/Simulink hardware-in-the-loop tool-chains. MATLAB's widespread use in aerospace curricula also makes it an effective educational and training platform. There are future plans to develop a version of FAST that is compatible with GNU Octave [†], a free programming language compatible with most MATLAB scripts, to make the code truly open-source.

FAST includes many pre-built aircraft models and mission profiles for a user to run before developing their own, thus reducing the time required to become a proficient user. Extensive documentation in the software package and a video tutorial series[‡] is available for users to quickly understand how to use FAST effectively.

This paper details the main features of FAST, how data-based and first-order physics-based models are combined to rapidly size an aircraft, and an example sensitivity study comparing an aircraft concept with different propulsion systems and operational strategies. The remainder of the paper is as follows. Section II highlights the main aircraft sizing and analysis features, and illustrates the inputs that a user must provide in order to analyze an aircraft. Section III describes the built-in regressions that estimate any unknown information about the candidate aircraft design using the Aerobase mentioned previously. Section IV describes the aircraft sizing process, including the workflow, assumptions, and simplifications made. Section V describes the energy-based mission analysis in detail and assumptions made in the segment analyses. Section VI outlines the gas turbine engine modeling included in FAST's propulsion system analyses. Section VII validates FAST using two conventional aircraft configurations. Section VIII demonstrates using FAST for a retrofit study on a commercial freighter aircraft. Section IX summarizes the work performed thus far and provides recommendations for further improving FAST.

II. Software Design and User Inputs

Before reviewing FAST's modules, a complete Design Structure Matrix (DSM) illustrating its computational procedure is provided in Fig. 1 (all DSMs in this paper were created using OpenMDAO [10]). All information that is fed-forward and fed-backward is denoted with the gray boxes in the DSM's upper and lower triangulars, respectively.

[†] https://octave.org/
[‡] https://dx.doi.org/10.7302/26047

Each dark blue cell groups certain functionalities together, which are also displayed in gray.

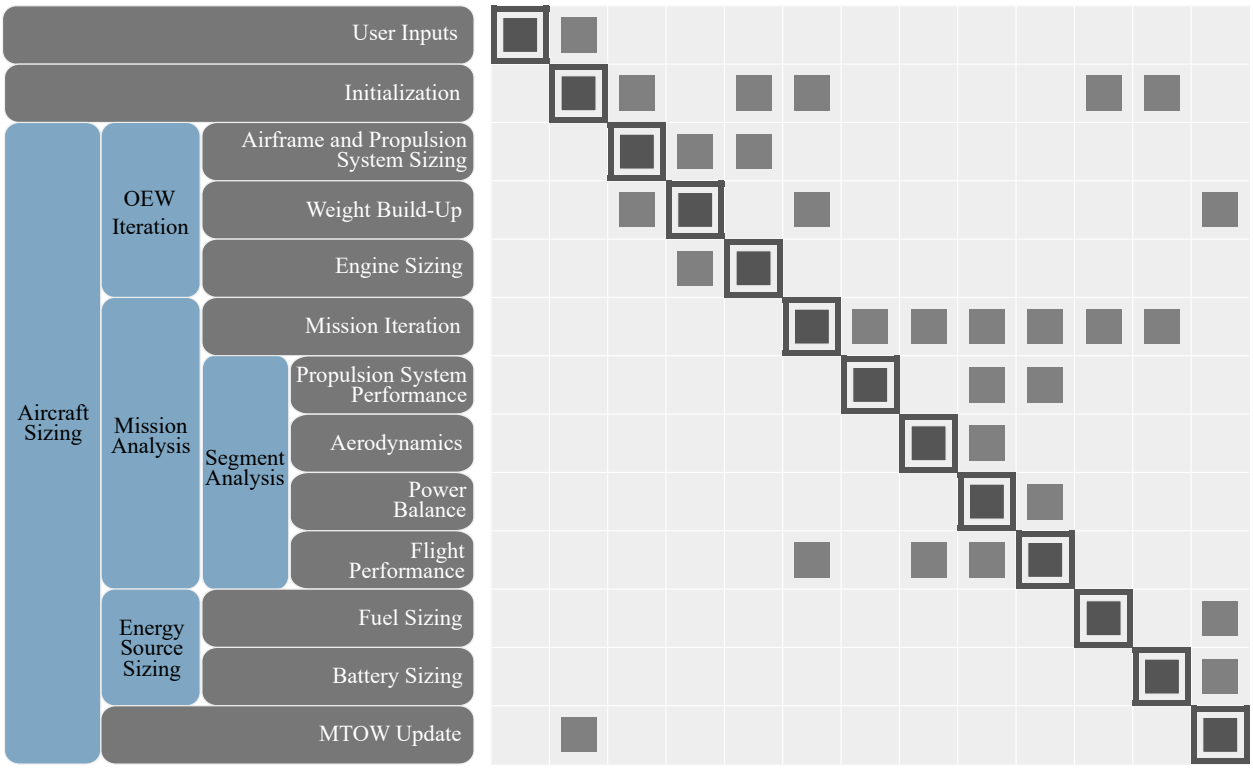

Fig. 1 FAST's overarching computational procedure.

There are three main components to FAST's software: 1) an "Initialization" module that processes the user inputs, identifies any unknown values, and estimates the unknown values using regressions from historical data; 2) an "Aircraft Sizing" module that uses a *fixed* set of point performance parameters to size the airframe and propulsion system; and 3) a "Mission Analysis" module that calculates the mission performance, including the energy required to fly the prescribed mission.

Two file inputs are required to analyze a configuration in FAST: 1) Aircraft Specification File; and 2) Mission Profile Specification File. The Aircraft Specification File lists all known design and performance parameters that describe the configuration and prescribes run settings (options) on how FAST should analyze the configuration. It also defines the propulsion system architecture and its operational strategies. FAST utilizes a matrix-based propulsion system analysis framework developed by Cinar et al. [24] to define the propulsion system architecture and operational strategies. The matrix-based framework allows the designer to easily change connections between components in the propulsion architecture and regulate power transfer between them. An example Aircraft Specification File is in Appendix X.A.

The Mission Profile Specification File describes the flight phases and trajectory flown while analyzing the configuration. Each mission profile is comprised of takeoff, climb, cruise, descent, and landing segments. These segments are allocated to one or more mission targets, a distance- or time-based value that the aircraft must fly. An

example Mission Profile Specification file is in Appendix X.A.

There are some key guidelines for developing mission profiles in FAST. The first and last segments of a mission profile may be a takeoff or landing segment, respectively. Additionally, an unlimited number of climb and descent segments may be included. Multiple cruise segments may be included in a mission profile. However, only one cruise segment can be allocated to each mission target. FAST uses a fixed point iteration to modify the cruise segment length until the mission target is attained. Therefore, FAST requires one free variable (the cruise segment length) to satisfy one constraint (the mission target).

A user could develop a more detailed mission analysis solver that allocates multiple cruise segments for a single mission target. FAST's flexible computational framework allows the user to replace portions of the analysis with their own, given that the inputs/outputs match those required by FAST.

III. Historical Data and Regressions

The Aircraft Specification File accepts over 50 inputs, but FAST only requires that four be provided – the aircraft class (turboprop or turbofan), number of passengers carried, design range, and propulsion architecture. This is because the user is not expected to know all of the aircraft's design parameters during early-phase conceptual design. All unknown aircraft performance and design parameters are predicted using the provided inputs and FAST's historical data regressions and technology projections (detailed in [22]). Figure 2 identifies where the regressions/projections are called within FAST's initialization routine. In this DSM, the: 1) orange cells represent user-prescribed inputs; 2) turquoise cell represents a major functionality in FAST and encapsulates all of its inputs (in dark green/blue) and outputs (in light green/blue).

The regressions are based on data from over 450 previously manufactured and flown aircraft, stored in the Aerobase. The data was gathered from: 1) Type Certificate Data Sheets (TCDS) published by the FAA and European Union Aviation Safety Agency; 2) Airport Planning Manuals; or 3) the aircraft manufacturer's website. Information about the aircraft's designation, engines, payload, flight envelope, fuel, dimensions, and cabin crew were all collected. Examples of the collected parameters include: certification date, number of installed engines, design range, maximum passenger capacity, maximum takeoff weight (MTOW), operational empty weight (OEW), maximum operational Mach Number, and wingspan. The information collected in the Aerobase drives the regressions to predict the design parameters for the aircraft design defined by the user. The regressions are created in real-time using Gaussian Process Models (GPMs), which utilize the aircraft's entry-into-service (EIS) year, design range, and maximum payload, other user-provided inputs. The GPM uses this information to create a regression and predict the unknown aircraft parameters, as explained by [22]. Some quantities that can be predicted by the regressions are the aircraft's MTOW, cruise flight conditions, thrust- or power-weight ratio, wing loading, and fuselage length. Also, during the aircraft sizing process, the regressions are used to estimate the airframe and propulsion system weights.

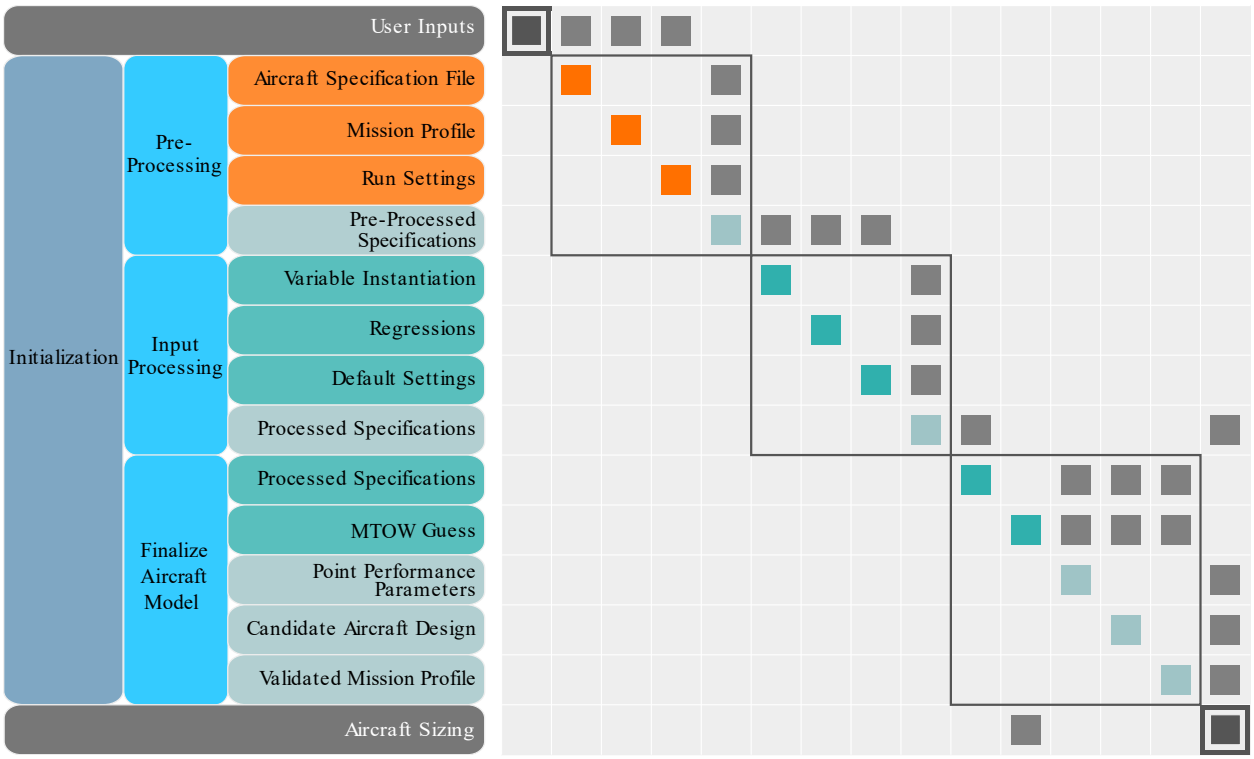

Fig. 2 FAST's initialization module.

Aside from the regressions, FAST also contains technology projections to predict key performance parameters associated with electrified aircraft components. The technology projections are represented by sigmoid curves, which predict the past, present, and future gravimetric specific energy for a battery and power-weight ratio for an electric motor. The projections only require two inputs – the aircraft's EIS year and its class (whether it is powered by a turbofan or turboprop engine). Aerodynamic, structural, and propulsive benefits for future technologies may be modeled in FAST. Given the wide range of technologies that could contribute to these disciplines, a unified scheme has not yet been implemented. Models for specific benefits, such as drag reduction due to boundary layer ingestion, should be developed based on the scope of the intended analysis. Wang et al. [25] exemplifies this by accounting for boundary layer ingestion and natural laminar flow effects in a model of NASA's SUSAN Electrofan concept in FAST.

IV. Aircraft Sizing

The aircraft sizing module predicts the airframe, propulsion system, and energy source (fuel, battery, etc.) weights. Its computational procedure is illustrated in Fig. 3. First, the "OEW Iteration" block sizes the airframe and propulsion system, followed by the mission analysis, which computes the required energy to fly the mission. Then, the "Energy Source Sizing" block determines the energy source weights.

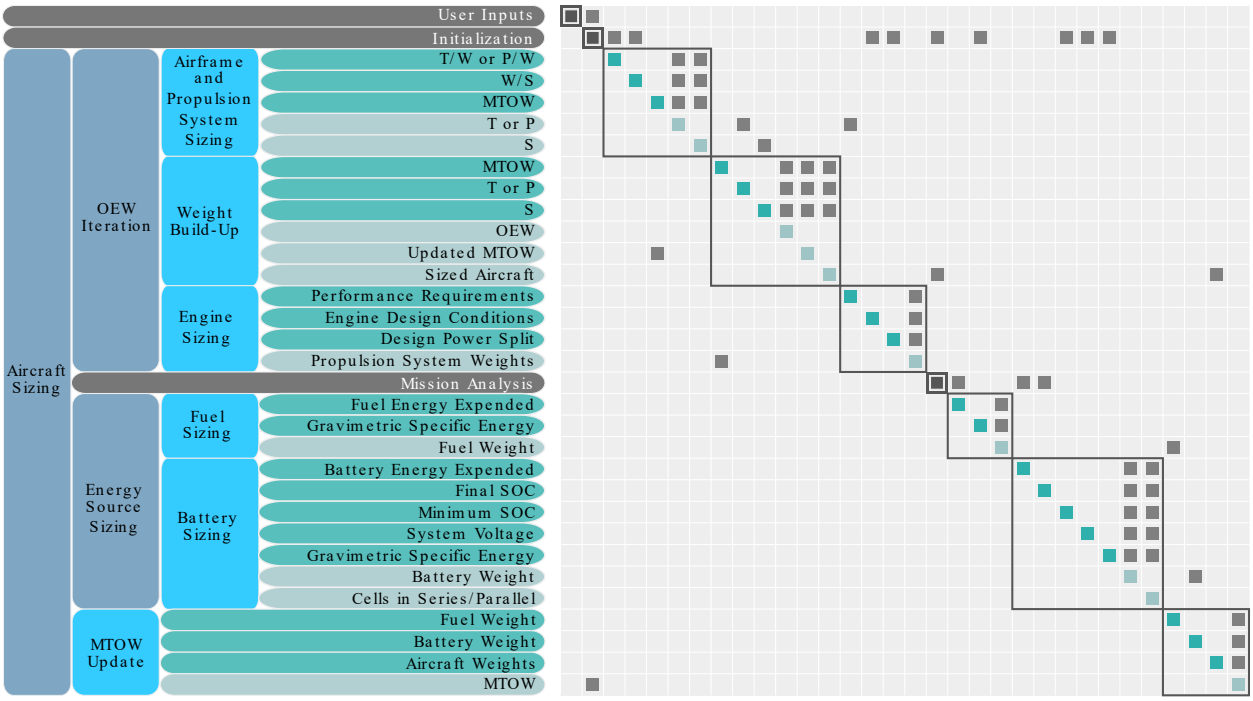

Fig. 3 FAST's aircraft sizing module.

A. Airframe and Propulsion System Sizing

The first sizing iteration estimates the airframe and propulsion system weights. A three-step process is used: 1) size the wing and propulsion system; 2) estimate the airframe and propulsion system component weights; and 3) update MTOW. FAST assumes that a feasible combination of point performance parameters (thrust- or power-weight ratio and wing loading) is provided by the user or the historical regressions.

FAST assumes that the point performance parameters *remain fixed* during sizing. Constraint diagram drawings are not yet integrated in FAST. The user may consider different thrust-/power-weight ratio and wing loading combinations to identify the optimum configuration, thanks to FAST's rapid analysis capabilities.

The user can couple their own constraint analysis into FAST by writing a script to re-analyze the design after dynamically updating the thrust-/power-weight ratio and wing loading in the Aircraft Specification File. Such an analysis could greatly impact the size of a novel concept, as certifying such configurations may require existing requirements to be modified or replaced entirely [26].

To size the wing, Eq. 1 is used, and is simply the quotient of MTOW and the wing loading. To size the propulsion system, the sea-level static (SLS) thrust (or power) is computed using Eq. 2 for turbofan aircraft or 3 for turboprop aircraft. The turbofan/turboprop engines are sized using a gas turbine engine model, as described in Section VI.

$$S = \text{MTOW} / \left(\frac{W}{S}\right) \tag{1}$$

$$\mathcal{T}_{\text{SLS}} = \left(\frac{\mathcal{T}}{W}\right) \text{MTOW} \tag{2}$$

$$P_{\text{SLS}} = \left(\frac{P}{W}\right) \text{MTOW} \tag{3}$$

After computing these values, the historical regressions estimate the airframe weight. For turbofan aircraft, a GPM predicts the airframe weight using the wing area, SLS thrust, EIS year, and MTOW. For turboprop aircraft, a linear regression predicts the airframe weight as a function of MTOW.

Next, the propulsion system components are sized. Recall that the SLS thrust/power was already computed using Eqs. 2 or 3. Using the respective values, each component in the propulsion system is sized based on the SLS thrust/power and design power splits provided by the user. The power splits are defined using the matrices developed by Cinar et al. [24]. After propagating the thrust/power to each component in the propulsion system, the component weights are estimated. A GPM predicts the turbofan or turboprop engine weights using its maximum SLS thrust or power, respectively. Electric motor weights are estimated using Eq. 4. The electric motor's power-weight ratio is either specified by the user, or estimated by the historical regressions/projections based on the EIS year provided.

$$W_{\text{EM}} = \frac{P_{\text{EM}}}{(P/W)_{\text{EM}}} \tag{4}$$

Lastly, the aircraft's MTOW is updated by adding the weights in Eq. 5 together. This sizing loop is a fixed point iteration [27], and repeats itself until converging on MTOW.

$$\text{MTOW} = W_{\text{Airframe}} + W_{\text{Propulsion System}} + W_{\text{Crew}} + W_{\text{Payload}} + W_{\text{Energy Sources}} \tag{5}$$

B. Energy Source Sizing

The energy source sizing is performed after the mission analysis and computes the fuel or battery that the aircraft must carry to fly the design mission. Two different approaches are used to estimate the weight of the fuel (energy-based) and battery (energy- and power-based).

1. Fuel Sizing

Fuel is defined as a substance that would be pumped into a storage tank on the aircraft, such as kerosene or hydrogen. The fuel weight is determined by dividing the energy expenditure during the design mission, E_{fuel}, by its gravimetric specific energy, e_{fuel}, as listed in Eq. 6. In other words, a fuel is only sized for its energy requirements.

$$W_{\text{fuel}} = \frac{E_{\text{fuel}}}{e_{\text{fuel}}} \tag{6}$$

Currently, the fuel sizing only considers the energy expenditure and neglects the weight of the fuel tanks. While this is a reasonable estimate for kerosene-powered aircraft, it may not be reasonable for hydrogen-powered aircraft, which require significantly heavier fuel tanks. As a remedy, the authors suggest adding a calibration factor greater than unity to the airframe weight to indicate that larger fuel tanks are necessary, thus making the airframe heavier.

2. Battery Sizing

The battery sizing accounts for both energy and power requirements. In FAST, a battery is built by arranging Lithium-ion cells in series (to obtain a desired system voltage) and in parallel (to obtain a desired power output). FAST assumes that each battery cell has a maximum capacity, Q_{max}, and maximum voltage, V_{max}, of 2.6 Ah and 3.6 V, respectively. FAST's modular computational framework enables users to substitute the default Lithium-ion battery cell model with alternative battery chemistries, or incorporate new (dis)charging models, provided the input/output structure remains consistent with FAST's current functions.

To run the battery sizing module, the user must specify the number of battery cells in series and in parallel as an initial guess in the Aircraft Specification File (defaults are used if none are provided). While sizing the aircraft, the number of battery cells in series remains fixed, corresponding to a fixed system voltage. However, the number of battery cells in parallel changes to satisfy the design mission's power demands. Unless otherwise specified by the user, the battery's initial state of charge (SOC) is assumed to be 100%. The battery is sized for the maximum power required during the mission and to ensure that its final SOC remains at or above 20%. A lower bound of 20% is applied because the battery could become permanently damaged if it is discharged any further [18].

While sizing the battery, two checks are performed. The first check determines whether the battery's final SOC is above/below the 20% threshold. Depending on the energy expenditure, the excess/lack of battery charge, ΔSOC, is computed to show how much energy must be added/removed from the battery. Then, Eq. 7 uses the existing battery capacity, Q_{batt}, and the SOC change to recompute the required number of cells in parallel [18]. To ensure that the number of battery cells remains an integer quantity, the brackets $\lceil$ and $\rceil$, are used represent the ceiling function, which rounds the result to the next largest integer.

$$N_{\text{par,SOC}} = \left\lceil \frac{Q_{\text{batt}} + (\Delta\text{SOC})\, Q_{\text{max}} N_{\text{par}}}{Q_{\text{max}}} \right\rceil \tag{7}$$

The second determines whether the maximum C-rate (battery discharge rate) is exceeded. The C-rate is defined in Eq. 8. FAST assumes a maximum C-rate of 5. If the maximum C-rate is exceeded, additional cells are added to ensure that the battery does not discharge too rapidly. Equation 9 is used to compute the requisite number of cells in parallel.

$$\text{C-rate} = \frac{\text{Power Required}}{\text{Total Energy}} \tag{8}$$

$$N_{\text{par,C-rate}} = \left\lceil \frac{\text{Maximum C-rate}}{\text{Maximum Allowable C-rate}} \right\rceil N_{\text{par}} \tag{9}$$

Using the values from Eqs. 7 and 9, the battery is resized using Eq. 10, which selects the number of cells in parallel based on the more demanding sizing requirement (ensuring a minimum 20% SOC or maximum allowable C-rate of 5) [18]. After identifying the number of parallel cells to be installed, the battery's weight is recomputed, as shown in Eq. 11. Note that N_{ser} represents the number of battery cells in series and e_{batt} represents the battery's gravimetric specific energy.

$$N_{\text{par,new}} = \max\left(N_{\text{par,SOC}}, N_{\text{par,C-rate}}\right) \tag{10}$$

$$W_{\text{batt,new}} = 3600 V_{\max} Q_{\max} N_{\text{ser}} N_{\text{par,new}} / e_{\text{batt}} \tag{11}$$

In some cases, the user may want to size the battery only for energy requirements, especially during early-phase conceptual design. If so, the battery sizing module can be skipped by excluding the number of battery cells in series and parallel from the Aircraft Specification File. Instead, the new battery weight ($W_{\text{batt,new}}$) is computed using Eq. 12, which solely depends on the battery's energy expenditure (E_{batt}) during the design mission.

$$W_{\text{batt,new}} = \frac{E_{\text{batt}}}{e_{\text{batt}}} \tag{12}$$

V. Mission Analysis

In the mission analysis, the user-prescribed mission profile is flown and computes the energy required to fly. The mission analysis informs the energy source sizing, as discussed previously in Section IV.B. Its computational procedure is illustrated in Fig. 4.

There are two sets of computations performed in the mission analysis: 1) the mission iteration; and 2) the segment analysis. The mission iteration performs a fixed-point iteration over the distance/time of the cruise segment allocated to each mission target. In the segment analysis, the aircraft flies the prescribed segments (takeoff, climb, cruise, descent, and landing) specified by the user. For this paper, the mission iteration is not discussed any further because it is not central to estimating the energy required to fly the mission. Instead, the computational procedure for the segment analysis and underlying assumptions within each segment are discussed in detail.

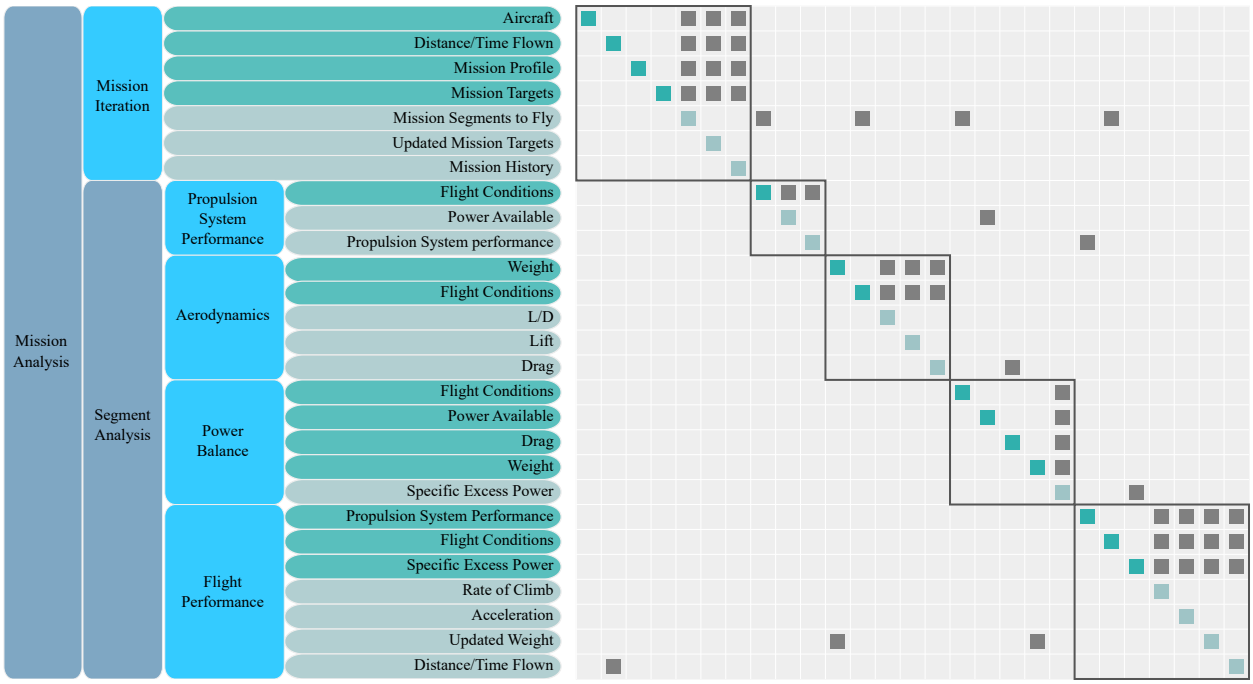

Fig. 4 FAST's mission analysis module.

A. Energy-Based Segment Analysis

In the energy-based segment analysis, the aircraft is assumed to be a point mass, neglecting all rigid body dynamics. The computational procedure used in the segment analysis follows Algorithm 1, located in Appendix X.B.

There are four main functionalities in the energy-based segment analysis: 1) propulsion system performance; 2) aerodynamics; 3) power balance; and 4) flight performance. The propulsion system performance module estimates the power available as a function of altitude. The aerodynamics module predicts the drag force on the aircraft, which is currently achieved by assuming a constant lift-to-drag ratio in each segment. The power balance module computes the available excess power to climb and/or accelerate. Lastly, the flight performance module computes the duration of each segment and returns the aircraft's rate of climb, acceleration, and energy expenditure. By assuming that the aircraft is a point mass, FAST's energy-based segment analysis can evaluate configurations with *any* propulsion architecture. This distinguishes it from previous work that developed propulsion architecture-dependent aircraft performance equations [12, 28].

As previously mentioned, five mission segments are available in FAST: 1) takeoff; 2) climb; 3) cruise; 4) descent; and 5) landing. Table 2 lists the assumptions made to simplify the analysis.

Future releases of FAST will contain more detailed segment analysis models that no longer rely on some of these assumptions. For example, the constant lift-to-drag ratio assumption could be removed by developing an elementary drag polar model. Additionally, more detailed takeoff and landing models that incorporate force balances would eliminate the

Table 2 Assumptions made in FAST's segment analyses.

Assumption	Takeoff	Climb	Cruise	Descent	Landing
Fixed Time	✓	✗	✗	✗	✓
Constant Acceleration	✓	✗	✗	✗	✓
No ISA Temperature Deviation	✓	✓	✓	✓	✓
Constant L/D	✗	✓	✓	✓	✗
Linearly Spaced Altitudes and Airspeeds	✓	✓	✓	✓	✓
Maximum Power	✓	✓/✗	✗	✗	✗
Reverse Thrust	✗	✗	✗	✗	✓

fixed takeoff/landing time assumptions.

B. Battery Discharge

FAST's battery (dis)charging model utilizes a Lithium-ion battery dynamics model, adapted from Tremblay and Dessaint [29]. This model is only utilized if the user specifies the number of battery cells in series and parallel. The battery dynamics model is shown in Eqs. 13 and 14. All parameters used in the model are listed in Tab. 3.

$$V_{\text{discharge}} = E_0 - Ri - K\frac{Q}{Q - it}\left(it + i^*\right) + Ae^{-Bit} \tag{13}$$

$$V_{\text{charge}} = E_0 - Ri - K\frac{Q}{it - 0.1Q}i^* - K\frac{Q}{Q - it}it + Ae^{-Bit} \tag{14}$$

Table 3 Variables used in the battery (dis)charging model.

Variable	Description
V	Battery voltage as a function of time (V)
E_0	Battery constant voltage (V)
R	Battery internal resistance (Ω)
it	Battery capacity as a function of time (Ah)
K	Polarization Constant (Ω)
Q	Maximum battery capacity (Ah)
i^*	Filtered current (A)
A	Battery's exponential zone amplitude (V)
B	Battery's time constant $\left(\text{Ah}^{-1}\right)$

Currently, only battery discharge is used in FAST. However, battery charging will be useful in the future for power management strategies that charge a battery from operating a gas turbine engine or windmilling from a propeller.

VI. Gas Turbine Modeling

A. Overview

FAST's engine modeling is a standalone feature that sizes and evaluates the performance of turbofan, turbojet, and turboprop engines. Figure 5 illustrates its computational procedure.

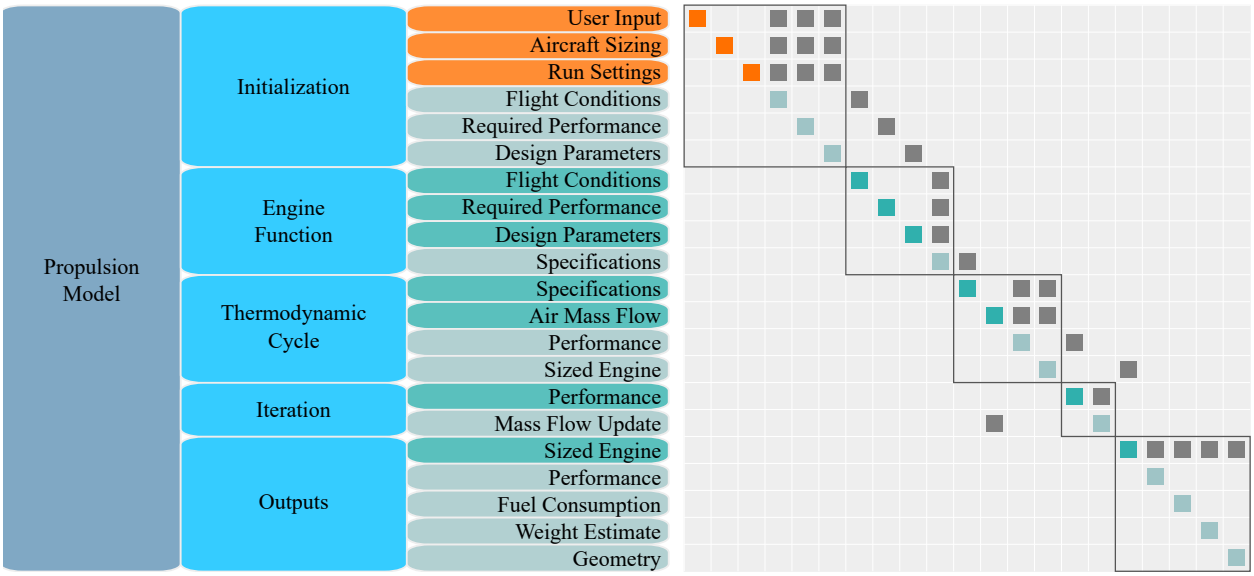

Fig. 5 Gas turbine sizing module within FAST.

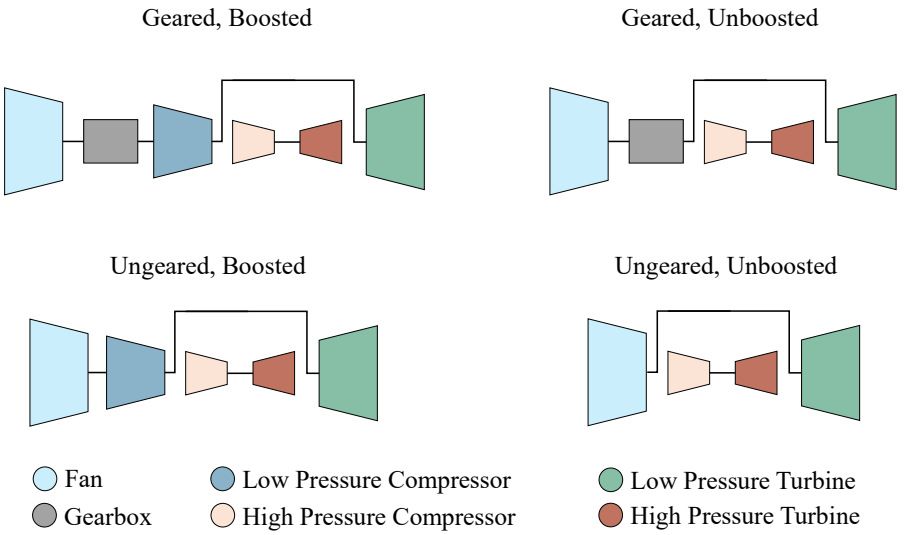

Fig. 6 Example architectures for a two-spool turbofan engine in FAST.

Similar to the aircraft sizing module, the gas turbine analysis requires a specification file to declare its design parameters, namely, the Engine Specification File (also a MATLAB script). This file must be manually constructed by the user without any `NaN` values, requiring the user to know (or guess) all information to size the gas turbine engine. The required design variables include the flight conditions and required thrust or power (turbofans or turboprops respectively) at the design point[§]. Information about the internal engine architecture (number of shafts, shaft speeds, gearing, etc.) is also required. Regressions from the Aerobase can assist users in this task, but the user must call them manually. Figure 6 provides examples of two-spool engine architectures that can be designed in FAST.

An engine can be included in an aircraft design by calling the Engine Specification File within the Aircraft Specification File. While sizing the aircraft, the engine's design parameters are held constant while the absolute size of the gas turbines are scaled until a desired thrust or power is produced at the engine sizing condition. As previously mentioned, FAST assumes takeoff thrust/power for the engine sizing condition. The required performance is calculated using the user provided thrust- or power-weight ratio and the current iteration MTOW. After converging on a sized engine, the regressions discussed in Sec. III are used to predict its weight and length.

Previously developed and validated engine models are included in FAST to provide examples of Engine Specification Files for the user. These include turbofans for regional (CF34-8E5), single aisle (LEAP-1A26, PW 1919G), and twin aisle class aircraft (Trent 970B-84), and turboprops for regional (PW 127M) and cargo (AE 2100-D3) aircraft. The engines' fuel consumption is calibrated using TCDS, manufacturer, or ICAO [30] values at its design thrust or power. Roux provides centralized data sourced from a variety of TCDS [31, 32]. For novel aircraft concepts, FAST scales these concepts to preserve their architectures while recalculating fuel flow at different flight conditions and sizing thrust or power demands. Off-design engine performance is discussed in Section VI.C.

B. Thermodynamic Cycle

The thermodynamic cycle within the gas turbine model follows the procedure(s) outlined in canonical sources including Mattingly [33], Boyce [34], Walsh and Fletcher [35], and Saravanamuttoo [36]. The cycle model calculates the power turbine output as a function of the air mass flow rate. A fixed point iteration on the air mass flow rate changes the engine size to generate the thrust/power requested by the user. A thermodynamic "flow state", comprised of values such as pressure, temperature, Mach Number, flow area, etc. is stored at each engine "station," illustrated by a station map shown in Tab. 4. This convention is shared between all types of gas turbine engines. If an engine does not have a component, it is simply ignored. For example, stations 1, 2, 2.1, 2.5, and 2.6 are identical for a turboprop engine with one compressor, as there is no fan, LPC, or IPC.

For some electrified propulsion architectures, an electrical power load may be requested/provided, thus increasing/re-

[§]During aircraft sizing, FAST assumes engines are sized at SLS conditions, using the thrust or power provided from the user-input thrust- or power-weight ratios. As a standalone feature, any flight condition can be used to size a gas turbine engine.

Table 4 FAST's engine station numbering convention.

Station Number	After	Before
0 or *a*	Streamtube	Inlet
1	Inlet	Fan
2	Fan	Splitter
2.1	Splitter (Core)	LPC
2.5	LPC	IPC
2.6	IPC	HPC
3	HPC	Bleed Air Extraction
3.1	Bleed Air Extraction	Combustion Chamber Diffuser
3.2	Combustion Chamber Diffuser	Combustion
3.9	Combustion	Turbine Diffuser
4	Turbine Diffuser	Cooling Air
4.1	Cooling Air	HPT
5	HPT	IPT
5.5	IPT	LPT
6	LPT	Core Nozzle
9	Core Nozzle	Core Exhaust
13	Splitter (Bypass)	Bypass Nozzle
19	Bypass Nozzle	Bypass Exhaust

ducing the power that the turbine must produce. FAST interprets positive electrical loads as a supplemental power boost (reducing the engine's power demands) and negative electrical loads as a supplemental power siphon (increasing the engine's power demands). Equation 15 shows this convention for turbines with known work requirements while Eq. 16 shows the same quantity for turbines with the goal of maximizing the power output. The left arrow represents that work done *on* the turbine is positive. To match this convention, a negative sign is included in front of the integral in Eq. 16 to ensure that the output of the integration from high to low temperature is positive. For example, a battery boosted takeoff would use a positive electrical work input, reducing turbine demand. In contrast, a turboelectric propulsion architecture would require a negative electric work input because the gas turbine engine is powering an electric generator, increasing turbine demand.

$$W_{\text{Turbine}} = \frac{W_{\text{Compressor}} - W^{\leftarrow}_{\text{Electrical}}}{\eta_{\text{Turbine}}} \tag{15}$$

$$W_{\text{Turbine}} = \frac{-\dot{m}_{\text{inlet}} \int_{T_{t,\text{inlet}}}^{T_{t,\text{exit}}} C_{p,\text{air}}(T) - W^{\leftarrow}_{\text{Electrical}}}{\eta_{\text{Turbine}}} \tag{16}$$

$$\text{where} \quad T_{t,\text{exit}} = T_{t,\text{inlet}}\left(\frac{P_{t,0}}{P_{t,4.1}}\right)^{\frac{\gamma-1}{\gamma}}$$

Turbine stage loading is limited to two, as suggested by Walsh and Fletcher [35]. The overall loading, ψ, is shown in Eq. 17, where ω is the turbine rotational velocity, R_p is the pitch line radius, $W_{\text{Compressor}}$ is the compressor work, and η_{Turbine} is the turbine efficiency. The number of required stages is computed by dividing the overall loading by the stage limit and rounding up to the nearest whole number.

$$\psi = \frac{W_{\text{Compressor}}}{\eta_{\text{Compressor}}(\omega R_p)^2} \tag{17}$$

After determining the number of stages, each one extracts energy from the airflow, "powering" the compressor and any additional electrical components requested by the propulsion architecture. Then, the design procedure depends on the engine being designed:

Turbofans: All turbines have a known work output, and use Eq. 15. After air passes through the turbines, the air in the core (and the bypass duct) is ideally expanded to atmospheric pressure at the design altitude, producing thrust described by Eq. 18, where all $\dot{m}$ are mass flow rates and all u are velocities.

$$\mathcal{T} = \dot{m}_9 u_9 + \dot{m}_{19} u_{19} - \dot{m}_0 u_0 \tag{18}$$

The thrust is output as the performance metric.

Turboprops/shafts: Eq. 15 is used for the turbines *except* if it is a free turbine, which uses Eq. 16. The work output from the free turbine is returned as the performance metric. If the turboshaft uses a single turbine to power both external thrust sources and its own compressor, the compressor work is subtracted from the turbine work before being returned as the output power.

The performance metric is output to the engine sizing iteration and the streamtube mass flow rate is modified until the computed performance matches that requested by the design specification and satisfies any additional electrical demands.

C. Off-Design Engine Modeling

This section details the engine's off-design performance analysis, and relies on a key assumption to predict the fuel consumption for turboprop/shaft engines in FAST: component efficiencies are constant with respect to the performance requirements and throttle settings. This yields a linear response in fuel consumption with respect to output power (constant brake-specific fuel consumption with respect to output power). The effects of these assumptions are offset by tuning a fuel flow calibration factor and comparing the total fuel burn to literature values at a design mission. Off-design

analysis for turbofans is discussed in Section VI.C.1.

For all engines, FAST must calculate the total power available from the gas turbines to ensure each mission segment is feasible for the given engine size. FAST currently uses an engine lapsing method presented in Anderson [37], and is described in Appendix X.B. This equation assumes the total thrust/power available from the engine is an exponential function of the density ratio. The exponent is set to one for turbofan engines and zero for turboprops/shafts, but may be modified by the user.

1. Off-design Turbofan Engine TSFC Model Overview

The following methodology only applies to turbofan engine analysis in FAST. The *International Civil Aviation Organization (ICAO) Aircraft Emissions Databank* provides comprehensive data on turbofan engine fuel flow rates across four operational modes, as reported by engine manufacturers [30]. The engine power settings available are at 100%, 85%, 30%, and 7%, representing the maximum power output for takeoff, climb-out, approach, and idle, respectively. Sun et al. [38] proposed a polynomial function for predicting the fuel flow rate under varying operational conditions. The polynomial function for each turbofan engine utilizes three coefficients, C_{ff3}, C_{ff2}, and C_{ff1}, derived from a third-degree polynomial curve fit of the points provided in the databank, shown in Eq. 19. Additionally, a simplified linear correlation factor, $C_{ff,ch}$, was introduced to account for discrepancies in the TSFC at SLS and cruise conditions at altitude, shown in Eq. 20. Combining Eqs. 19 and 20, the final fuel flow rate equation is provided in Eq. 21.

$$\dot{m}_{f,\text{ICAO}}\left(\mathcal{T}\right) = C_{ff3}\left(\frac{\mathcal{T}}{\mathcal{T}_0}\right)^3 + C_{ff2}\left(\frac{\mathcal{T}}{\mathcal{T}_0}\right)^2 + C_{ff1}\left(\frac{\mathcal{T}}{\mathcal{T}_0}\right) \tag{19}$$

$$\begin{aligned} C_{ff,ch} &= \frac{\text{TSFC}_{\text{Cr}} - \text{TSFC}_{\text{SLS}}}{h_{\text{Cr}}} \\ &= \frac{\text{TSFC}_{\text{Cr}} - \dot{m}_{f,\text{ICAO}}\left(\mathcal{T}_0\right)/\mathcal{T}_0}{h_{\text{Cr}}} \end{aligned} \tag{20}$$

$$\dot{m}_f\left(\mathcal{T}, h\right) = C_{ff3}\left(\frac{\mathcal{T}}{\mathcal{T}_0}\right)^3 + C_{ff2}\left(\frac{\mathcal{T}}{\mathcal{T}_0}\right)^2 + C_{ff1}\left(\frac{\mathcal{T}}{\mathcal{T}_0}\right) + C_{ff,ch} \times \mathcal{T} \times h \tag{21}$$

In these equations, $\dot{m}_{f,\text{ICAO}}(\mathcal{T})$ represents the fuel flow rate of an engine provided in the ICAO databank (in kg/s); $\mathcal{T}$ and $\mathcal{T}_0$ represent the required thrust during flight and the maximum static thrust of the engine (kN), respectively; TSFC_{Cr} and TSFC_{SLS} represent the thrust specific fuel consumption for cruise and sea-level conditions, respectively; and h_{Cr} represents the aircraft's cruise altitude.

2. Turbofan Engine TSFC Model Validation

The fuel flow equation presented in Eq. 21 was validated by estimating the coefficients in Eqs. 19 and 20 using data from the ICAO databank and relevant literature [30, 39, 40], as detailed in Appendix X.C. Four turbofan engines from different manufacturers were selected to demonstrate the accuracy of the third-degree polynomial curve fitting results compared to the ICAO databank, shown in Fig. 7. The engines are the CF34-8E5, LEAP1A26, LEAP1B and Trent 772, which are used on the Embraer ERJ175LR, Airbus A320neo, Boeing 737 Max 8 and Airbus A330, respectively. As shown in Fig. 7, the fuel flow results derived from the curve fits closely match the values in the ICAO databank, with the exception of low thrust conditions, such as idle. During the design mission, the engine operates at low thrust regimes for only a brief period of time, and the fuel consumption at these points is negligible relative to the total block fuel. As a result, the overall block fuel is not significantly impacted by this discrepancy.

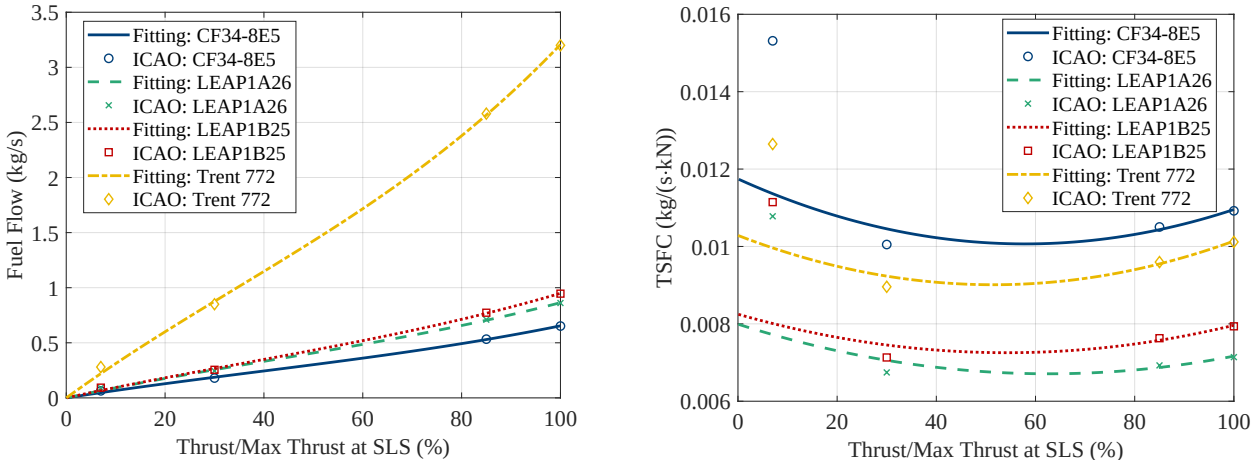

(a) Fuel flow data. **(b) TSFC data.**

Fig. 7 Curve fit validation against the ICAO databank.

The simplified linear correlation factor was calculated using Eq. 20 and relevant cruise TSFC data [38–40]. Appendix X.C provides these coefficients for 32 turbofan engines. Although the Aerobase includes many turbofan engines with C_{ff3}, C_{ff2}, and C_{ff1} values, only 32 of them have corresponding $C_{ff,ch}$ values due to the lack of publicly available TSFC data. For any engines not presented in Appendix X.C, an average $C_{ff,ch}$ of 6.8×10^{-7} is assumed and used in FAST.

After implementing these equations in FAST, an Embraer ERJ175LR [41] with the CF34-8E5 engine [39] and an Airbus A320neo [42–44] with the LEAP1A26 engine [40] were selected to examine whether the function accurately estimates the fuel consumption for their respective design missions in FAST. Table 5 lists a comparison between multiple aircraft performance parameters estimated in FAST and their literature values. The percent errors are less than 2% by tuning the fuel flow rate, airframe weight, and the lift-to-drag ratio in climb/cruise. Therefore, these results demonstrated the turbofan off-design engine modeling in FAST has the capability to accurately estimate the performance of sized

aircraft.

Table 5 Validated aircraft models using FAST's off-design engine analysis capability.

Parameter	ERJ175LR			A320neo (Weight Variant 054)		
	FAST	Literature	Difference	FAST	Literature	Difference
MTOW (kg)	38,637	38,790	-0.39%	79,333	79,000	+0.42%
OEW (kg)	21,545	21,500	+0.21%	44,581	44,300	+0.63%
Block Fuel (kg)	9,397	9,428	-0.33%	18,856	18,729**	+0.68%
Cruise TSFC (lb/lbf/hr)	0.692	0.680	+1.76%	0.514	0.51	+0.78%

**Values range from 18,729 to 21,005 kg depending on factors such as the number of fuel tanks installed, passenger capacity, weight variant, etc. In this case, the FAST inputs for this design point reflect an A320neo without the additional center fuel tank.

VII. Validation: Notional Aircraft Sizing

FAST is validated by sizing two notional aircraft models representative of an Airbus A320Neo [43, 44] and Embraer E175LR [41, 45]. Parameters were gathered from publicly available type certificate data sheets and airport planning manuals. Key performance and design parameters for each aircraft are listed in Tab. 6.

Table 6 Key performance and design parameters for validating FAST.

Parameter	Airbus A320Neo	Embraer E175LR
Passengers	160	78
Class	Turbofan	Turbofan
Entry into Service	2016	2005
Design Range [nmi]	2,600	2,150
Cruise Speed [Mach]	0.82	0.78
Cruise Altitude [ft]	35,000	35,000
Takeoff Speed [kts]	135	135
Maximum Rate of Climb [ft/min]	2,250	2,250
Climb/Descent L/D	16.00	10.98
Cruise L/D	18.23	15.20
Wing Loading [lbm/ft^2]	127.9	109.3
MTOW [lbm]	174,170	85,517
Block Fuel [lbm]	41,890	20,785
Operational Empty Weight [lbm]	93,917	47,399
Engine	LEAP 1A-26	CF34-8E5
Thrust-Weight Ratio	0.3287	0.3393
Cruise SFC [lbm/(lbf-hr)]	0.510	0.680

Each aircraft was sized in FAST using the previously provided specifications and a mission profile unique to each aircraft, listed in Appendix X.D. Table 7 lists the (un)calibrated performance parameters output by FAST. The

uncalibrated models illustrate the accuracy and robustness of the data-based models included in FAST. The calibrated models were developed by adjusting four factors – airframe weight scale factor, fuel flow scale factor, cruise lift-to-drag ratio, and climb/descent lift-to-drag ratio – to match the MTOW, block fuel, and OEW provided in the literature. The calibration factors used to achieve these results are listed in Appendix X.D.

Table 7 Conventional aircraft validation in FAST.

Weight	**Notional A320Neo**		**Notional ERJ175LR**	
	Uncalibrated	**Calibrated**	**Uncalibrated**	**Calibrated**
MTOW [lbm]	165,028	170,927	79,455	85,179
	(-5.25%)	(-1.86%)	(-7.09%)	(-0.40%)
Block Fuel [lbm]	38,112	41,896	19,580	20,717
	(-9.02%)	(+0.01%)	(-5.80%)	(-0.33%)
OEW [lbm]	91,872	93,988	42,912	47,499
	(-2.18%)	(+0.08%)	(-9.47%)	(+0.21%)
Cruise SFC [lbm/(lbf-hr)]	0.514	0.551	0.697	0.670
	(+0.78%)	(+8.04%)	(+2.50%)	(-1.47%)
Cruise Thrust [kN]	20.02	20.51	11.29	11.99

Both MTOW and block fuel are slightly underestimated because FAST slightly under-predicts the cruise thrust, requiring less fuel to fly. As a result of the block fuel decrease, MTOW also decreases and the aircraft design converges to a smaller size.

The underestimation is due to a combination of assumptions made in FAST. First, the mission analysis uses a constant lift-to-drag ratio in each mission segment. This assumption sacrifices accuracy for computational efficiency, particularly for the climb and descent segments when the aircraft may be flying with flaps partially/fully extended. Implementing a more detailed drag polar model would improve the accuracy while sacrificing computational efficiency, but also require information about the aircraft's geometry. Second, the regression-based weight estimation tends to slightly under-predict the airframe weight [22]. This also results in a lighter aircraft that requires less fuel to fly. Using a regression-based weight estimate is less computationally demanding than a physics-based weight estimate and also allows the user to design an aircraft with little known information about it.

Overall, the assumptions made are useful to simplify the analysis while sacrificing little accuracy, especially while exploring various configurations at the onset of conceptual design. FAST's modular framework allows any user to include more detailed models, as long as their inputs/outputs match those required in the computational framework.

VIII. Case Study: A Notional Electrified Freighter

FAST's ability to rapidly explore the design space and perform high-level trade studies is demonstrated using a notional model of Lockheed Martin's LM100J, a commercial freighter aircraft, depicted in Fig. 8 [46]. This aircraft was

used in prior NASA studies [47, 48], which included designing a variety of electrified freighters with varying range and payload requirements to identify ones that burned less fuel relative to the conventional configuration.

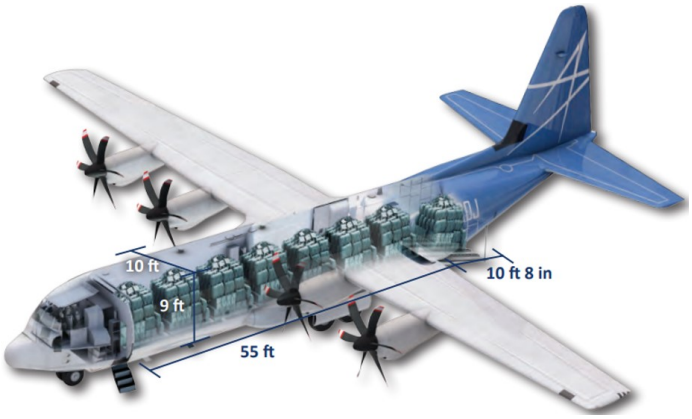

Fig. 8 LM100J freighter aircraft.

This case study explores how the electrified aircraft's fuel burn is impacted by different electrification technologies and operational strategies, and answers the following research question: for an independent parallel hybrid electric aircraft, what are the sensitivities of the block fuel with respect to the battery specific energy and the percentage of payload removed from the aircraft to accommodate an electrified propulsion system?

The independent parallel hybrid propulsion architecture is depicted in Fig. 9. Each outboard propeller is connected to its own electric motor. For simplicity, it was assumed that one battery provides the power required to operate both electric motors. The expression above each green arrow represents the fraction of thrust provided by each propeller, and is defined by λ, the thrust split, in Eq. 22.

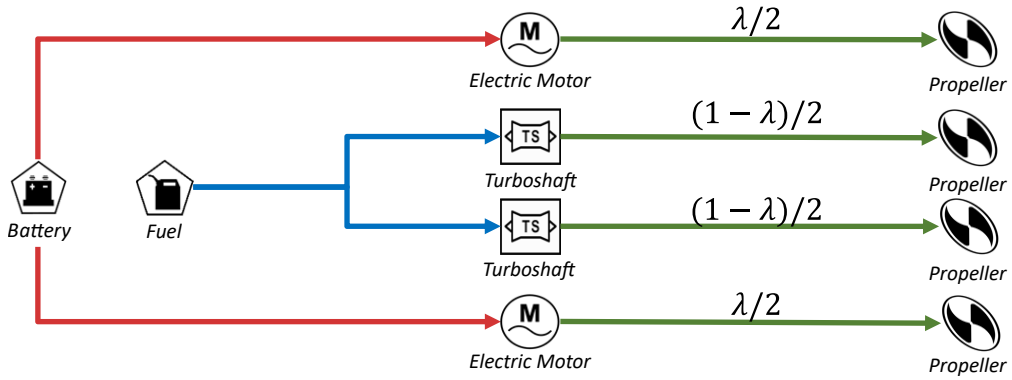

Fig. 9 Electrified propulsion architecture for the freighter.

$$\lambda \equiv \frac{\text{Total Thrust Provided by the Outboard Propellers}}{\text{Total Thrust Required}} \tag{22}$$

The case study is executed in two steps. First, a notional LM100J model is sized in FAST as a baseline. Second, a variety of freighters are designed by retrofitting the baseline airframe with an electrified propulsion system. This involves installing turboshaft engines and electric motors sized for a given thrust split, and replacing part of the payload with a battery to power the electric motors.

A. Conventional Freighter Modeling

The conventional freighter's performance parameters, shown in Tab. 8, were estimated from the LM100J's TCDS [49] and Lockheed Martin's informational pamphlet [46]. The aircraft flies a 2,390 nmi design mission, cruising at 25,000 ft and Mach 0.59. A 45-minute loiter at 10,000 ft and 300 KTAS was added as a reserve mission to properly estimate the block fuel.

Table 8 LM100J aircraft specification and performance parameter estimates.

Parameter	**Units**	**Value**
Design Range	nmi	2,390
Payload	lbm	40,000
Power-Weight Ratio	W/kg	183.4
Wing Loading	lbm/ft^2	123.7
MTOW	lbm	164,000
OEW	lbm	80,350
Block Fuel	lbm	38,000
Cruise Speed	Mach	0.59

Using the performance parameters and mission profile, the conventional freighter model was calibrated in two steps. First, the turboprop engine was tuned to match the cruise SFC from literature [31] by adjusting the engine's total burner temperature and polytropic efficiencies. Second, four other factors – airframe weight scale factor, fuel flow scale factor, cruise lift-to-drag ratio, and climb/descent lift-to-drag ratio – were adjusted to match the MTOW, block fuel, and OEW given in Tab. 8 as closely as possible without deviating from the baseline significantly. To prevent this deviation, all calibration factors were required to remain within 10% of unity. As a result of the constant lift-to-drag ratio assumptions and data-based weight estimations, it is not guaranteed that the MTOW, block fuel, and OEW will exactly match those in the literature. The tuned parameters are listed in Tab. 9.

The corresponding weights from the calibrated freighter model are provided in Tab. 10. Since this case study focused on reducing the freighter's fuel burn, the parameters were tuned to most closely match the block fuel. Overall, the calibrated model closely predicts the published values for the LM100J.

Table 9 Parameters tuned to calibrate the conventional freighter model.

Parameter	Value
Airframe Weight Scale Factor	0.991
Engine Fuel Flow Scale Factor	1.037
Cruise L/D	14.850
Climb/Descent L/D	12.850
Total Burner Temperature (K)	1,200
Inlet Polytropic Efficiency	0.990
Diffuser Polytropic Efficiency	0.990
Compressor Polytropic Efficiency	0.860
Combustor Polytropic Efficiency	0.980
Turbine Polytropic Efficiency	0.860
Nozzle Polytropic Efficiency	0.985

Table 10 Comparison between the notional LM100J and the literature.

Weight	Notional LM100J	Literature	Percent Error
MTOW (lbm)	159,953	164,000	-2.470%
OEW (lbm)	80,333	80,350	-0.021%
Block Fuel (lbm)	38,001	38,000	+0.003%

B. Retrofit Procedure

The baseline model was then retrofitted with the independent parallel hybrid propulsion architecture. The electric motors were assumed to have a 10 kW/kg power-weight ratio, similar to that of a prior study (9.85 kW/kg) [47]. The calibration factors established while tuning the baseline model remain constant for all system-level assessments to ensure that only the new technologies and operational strategies impact the following results.

The electrified freighter was retrofit using the computational procedure outlined in Fig. 10. First, a fraction of the payload is removed from the aircraft to accommodate the electrified systems, re-sized turboshaft engines, and electric motors. Then, a fixed point iteration is used to compute the fuel and battery weights required to fly. This involves flying the design mission to determine the requisite fuel and then allocating any remaining weight to the battery such that the electrified freighter's takeoff gross weight (TOGW) matches its MTOW. The design mission is flown a constant thrust split until the battery is fully depleted. After battery depletion, the outboard propulsors are turned off and only the inboard propulsors power the aircraft.

C. System-Level Assessments

The system-level assessments involve varying the battery technology and operational strategies. Table 11 lists the three design variables and their bounds. The payload removed and battery specific energy are treated as continuous

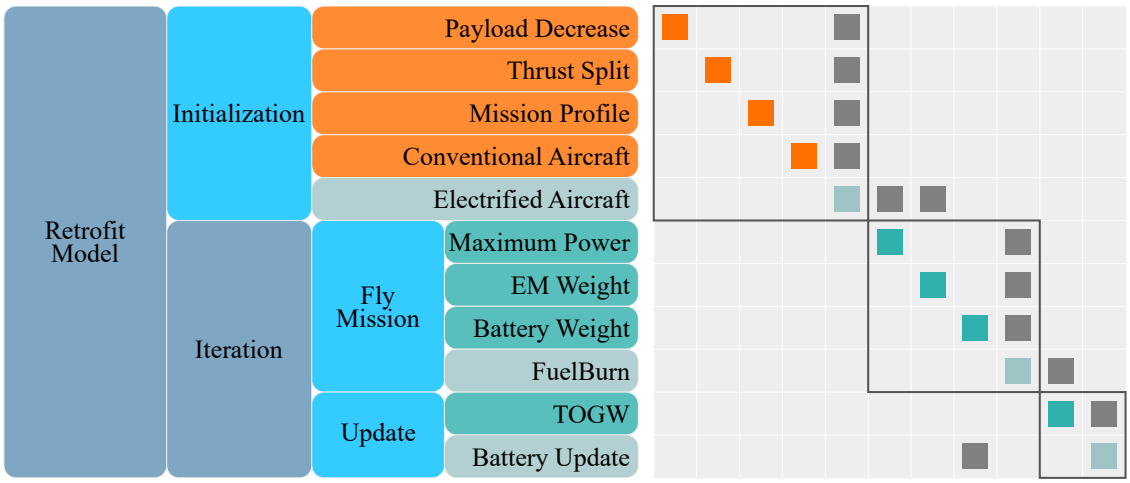

Fig. 10 Computational procedure for retrofitting an aircraft in FAST.

variables. The thrust split is treated as a discrete variable and is sampled in 10% increments.

Table 11 Design space for retrofit study.

Parameter	Units	Lower Bound	Upper Bound
Payload Removed	%	0	100
Thrust Split	%	10	30
Battery Specific Energy	kWh/kg	0.35	1.55

The electrified freighter's fuel burn is compared to that of the baseline aircraft flying two different payloads. The first comparison is against the baseline carrying a full payload, resulting in the same TOGW as the electrified configuration. Comparing these two aircraft answers the question: "How much fuel can be saved if payload is sacrificed for an electrified propulsion system?" The second comparison is against the baseline carrying the same payload as the electrified one, resulting in a smaller TOGW. This comparison quantifies the impacts of the weight penalty associated with electrifying the aircraft's propulsion system and answers the question: "Are the fuel savings from the electrified aircraft better than simply reducing the payload carried by the conventional aircraft?" In this study, it is assumed that both aircraft fly at the same lift-to-drag ratios during the mission.

A notional weight breakdown of each comparison aircraft is shown in Fig. 11. The left bar represents the conventional aircraft flying at the same TOGW as the electrified aircraft. The center bar represents the conventional aircraft carrying the same payload as the electrified aircraft, but flying at a smaller TOGW. The right bar represents the electrified aircraft.

The following figures contain results from the retrofit study. In these figures, the left plot represents the block fuel change between the conventional and electrified aircraft flying at the same MTOW (the left and right bars in Fig. 11). The right plot represents the block fuel change between the conventional and electrified aircraft carrying the same

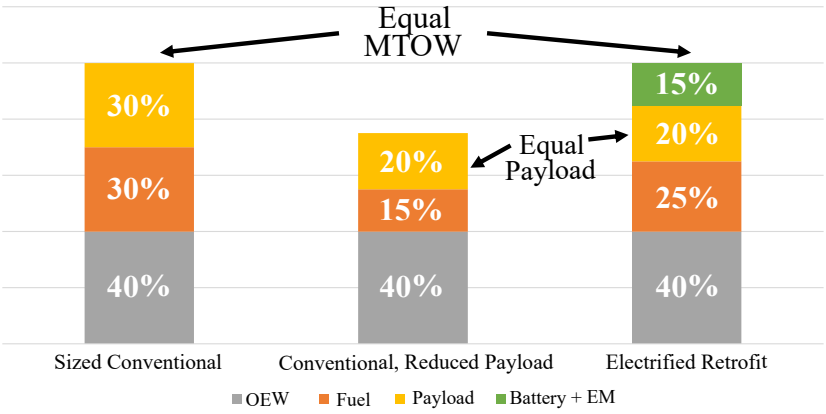

Fig. 11 Notional weight breakdown of aircraft compared in the retrofit study.

payload (the center and right bars in Fig. 11). Also, the bounds of the horizontal and vertical axes represent the bounds of battery specific energy and payload removed, respectively, provided in Tab. 11.

Figure 12 shows contours of the block fuel change between the conventional and electrified freighter for a 10% thrust split. Figure 12a illustrates that electrifying the aircraft at the same MTOW always saves fuel. For small percentages of payload removed, a 1 to 5% fuel savings is achieved, regardless of the battery specific energy. If larger percentages of the payload are removed, then a greater fuel savings (between 5 to 9%) is achieved. However, this is not desirable because the electrified freighter is carrying much less payload than its conventional counterpart.

Also, the contours of constant fuel burn change are steeper for lower battery specific energies. This suggests that improving the battery technology will have a greater impact on the fuel burn savings than removing payload from the aircraft. Conversely, once the battery technology matures (and grows to be between 1.0 and 1.5 kWh/kg), the contours of constant fuel burn change are less steep. Then, it is more beneficial to remove payload from the aircraft instead of improving the battery technology. However, this is not desirable from an aircraft operations perspective because less cargo is being carried.

Figure 12b reveals that electrifying the aircraft and carrying the same payload requires more fuel to be burned for most configurations. This is due to the weight penalty from electrifying the propulsion system – the battery and electric motors increase the aircraft's TOGW. Some combinations of battery specific energy and payload decrease in the lower right-hand corner of the plot save little fuel. However, this is for higher battery specific energy values that have not yet been attained.

Despite the weight penalty imposed by the electrified system, an interesting behavior emerges. At some point, the contours of constant block fuel change become horizontal, and are marked with the white dashed line. The horizontal lines indicate that the block fuel required to fly the mission is constant, regardless of the battery technology available. This suggests that the thrust split is too low and the battery is not being fully deplete. Otherwise, the block fuel change

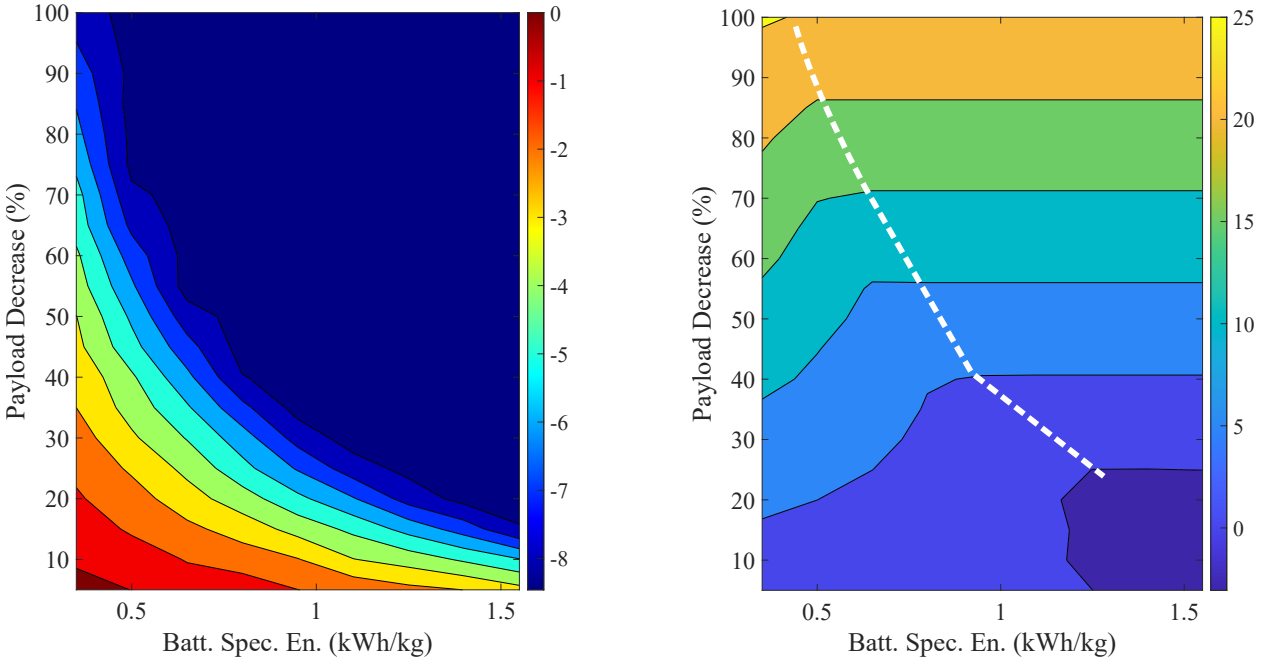

(a) Equal MTOW. **(b) Equal payload.**

Fig. 12 Block fuel change, 10% thrust split.

would improve for larger battery specific energy values. In these cases, part of the battery carried is "dead weight" and is not expended during the mission. To fully reap the benefits of electrifying the propulsion system, the aircraft should be operated at a higher thrust split.

Figure 13 shows contours of the block fuel change between the conventional and electrified freighter for a 20% thrust split. Figure13a illustrates that fuel is saved by increasing the battery specific energy and removing payload. However, there are some cases with no fuel burn savings, particularly in the lower left-hand corner of the plot. Since the electric motors doubled in size (relative to the ones used for a 10% thrust split), the battery became smaller to accommodate the larger electric motors and ensure that MTOW is not exceeded. Therefore, the battery supplied energy to the electrified aircraft for a much shorter period of time, and more fuel was needed to fly the mission. Similar to the results for a 10% thrust split, the contours of constant block fuel change are steeper for smaller battery specific energy values. The contours of constant block fuel change are not as steep for larger battery specific energy values. Again, this implies that the best way to save fuel is by improving the battery technology rather than removing payload from the aircraft.

Figure 13b reveals similar results as shown while operating the electrified freighter at a 10% thrust split. For most missions, more fuel was required due to the weight penalty associated with electrifying the propulsion system. Lines of constant block fuel change are still horizontal for larger battery specific energy values, indicating that not all of the battery is used while flying the mission. Towards a battery specific energy of 1.5 kWh/kg, an interesting point emerges, and is denoted with a white dot in Fig. 13. Beyond this point, increasing the battery specific energy allows the designer

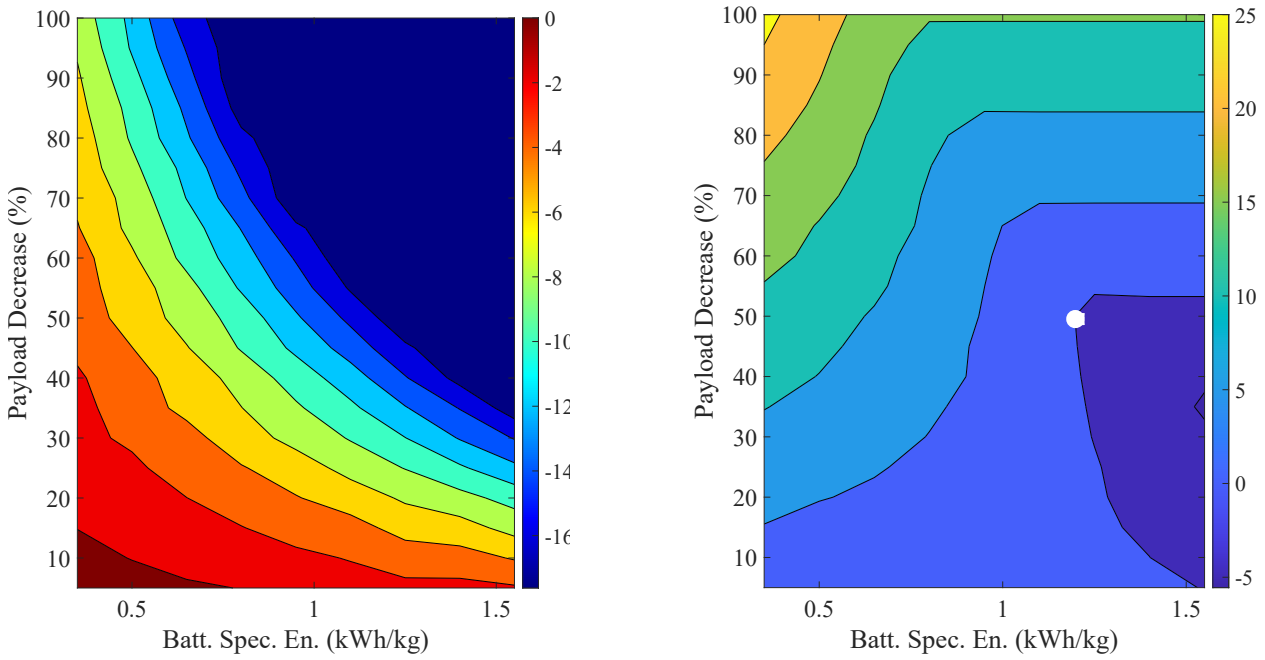

(a) Equal MTOW. **(b) Equal payload.**

Fig. 13 Block fuel change, 20% thrust split.

to add payload back into the aircraft. This is reflected by the contour with a negative slope underneath the point of interest – increasing the battery specific energy and adding payload back into the aircraft burns the same amount of fuel as the white point. This is desirable because more payload can be carried by the aircraft, as long as the battery specific energy continues to improve. Conversely, another part of the contour above the point of interest has a positive slope – increasing the battery specific energy and removing more payload burns the same amount of fuel as the white point. From an operational perspective, this is undesirable because the battery is too heavy and will not be fully used during the mission.

Lastly, Fig. 14 shows contours of the block fuel change between the conventional and electrified freighter for a 30% thrust split. Figure 14a illustrates that fuel is saved by increasing the battery specific energy and removing payload. Again, there are more combinations of payload removed and battery specific energy in the lower left-hand corner that do not exhibit any fuel burn savings. This is because the electric motors have tripled in size (relative to the electric motors sized for the 10% thrust split) and the battery onboard must become smaller to ensure that the electrified aircraft does not exceed MTOW. Also, the slopes of the contours are similar to the previous cases, but are less steep at lower battery specific energy values. This suggests that, for higher thrust splits, removing payload or improving the battery specific energy has the same impact on the fuel burn savings.

In Fig. 14b, more fuel is required to fly the mission due to the weight penalty imposed by the electrified propulsion system. Lines of constant block fuel change still exist, but only for cases in which nearly all of the payload is removed

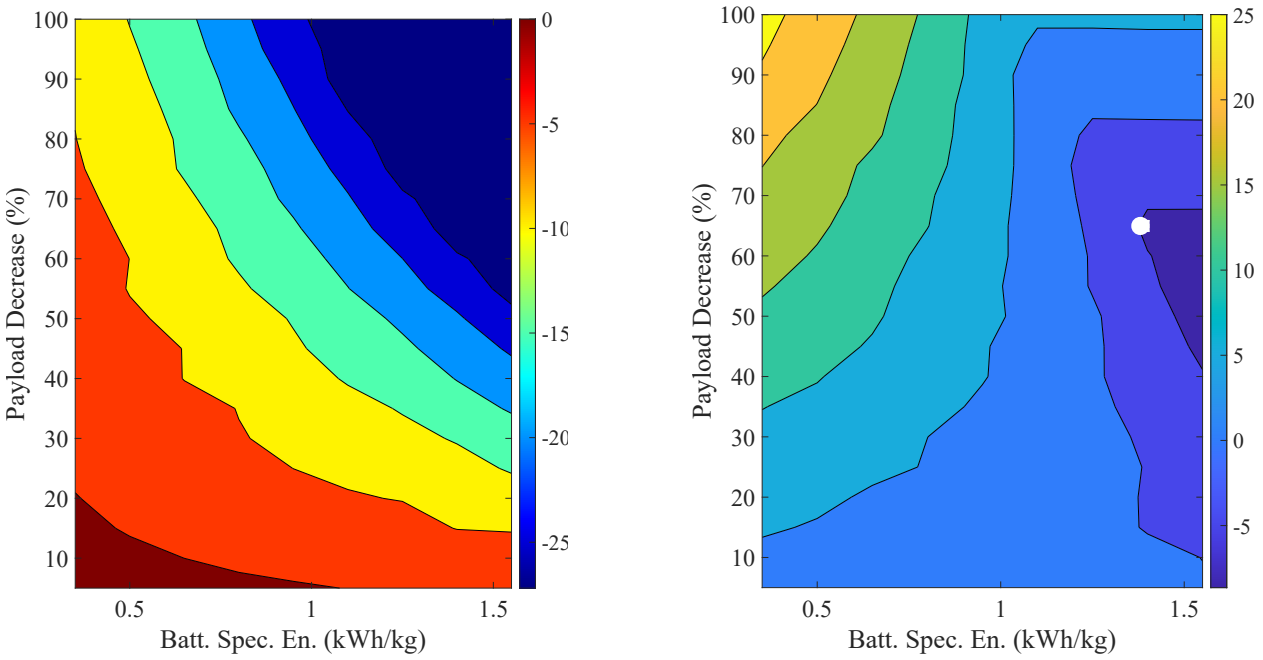

(a) Equal MTOW. **(b) Equal payload.**

Fig. 14 Block fuel change, 30% thrust split.

from the electrified freighter, which is not operationally desirable. Again, a critical point emerges (white point) – the contour of constant block fuel change has both a positive slope and negative slope as the battery specific energy increases. As previously mentioned, following the contour with a negative slope is more desirable because payload is added back into the aircraft as the battery specific energy improves. This makes the electrified freighter a more operationally viable alternative to a conventionally gas turbine powered freighter jet. Also, towards a battery specific energy of 1.25 kWh/kg, the slope of the contours change from positive to negative. This indicates that there is a critical battery specific energy that will provide the same block fuel change regardless of how much payload is removed. Additional work is needed to quantify this point and further explore its ramifications.

IX. Conclusions and Future Work

The Future Aircraft Sizing Tool (FAST) provides an advanced, open-source platform for early-phase conceptual design across a range of propulsion architectures, including electrified configurations. FAST distinguishes itself with several novel capabilities:

1) **Propulsion-agnostic design flexibility:** FAST accommodates a wide range of propulsion architectures without requiring specific propulsion dependencies, enabling comparative analysis across architectures, such as hybrid-electric, fully electric, and conventional designs.
2) **Integrated engine modeling:** Unlike many aircraft sizing tools that rely on external models or engine decks,

FAST incorporates a built-in engine model capable of directly sizing and simulating turbofan, turbojet, and turboprop engines without predefined engine performance decks. This feature allows FAST to dynamically evaluate fuel consumption, thrust, and efficiency under varied mission conditions.

3) **Rapid, integrated aircraft sizing and performance analysis:** The tool's fast convergence (typically under one minute) facilitates iterative design exploration, even for complex propulsion configurations.
4) **Historical aircraft database and data-driven modeling:** Leveraging a dataset of over 450 historical aircraft, FAST integrates data-driven models for accurate initial parameter estimations, which support early-phase design efforts when complete specifications may be unavailable.
5) **Energy-based mission analysis:** FAST applies an energy-based mission analysis approach, enabling flexible assessment across diverse mission profiles and making it particularly well-suited for evaluating energy-sensitive configurations like electrified aircraft.

FAST's capabilities make it an effective tool for design space exploration and sensitivity analysis, addressing the current need for flexible, propulsion architecture-independent tools that support emerging technologies in aviation. The source code for FAST is freely available on GitHub[¶].

FAST's capabilities were showcased by electrifying a commercial freighter by powering its outboard propellers with electric motors. A portion of the payload was removed to allocate space for the battery, as the added weight of the electrified system increased the aircraft's takeoff gross weight. In the first retrofit study, the electrified freighter's TOGW matched the MTOW of the conventional aircraft. These results indicated that improving the battery specific energy has a more significant impact on fuel savings than further payload reduction. Specifically, the battery technology must mature to very high specific energy levels (1.0-1.5 kWh/kg) for potential fuel savings to become substantial without additional payload sacrifices. With lower battery-specific energy values (up to 0.60 kWh/kg for a 10% thrust split and 0.75 kWh/kg for a 20% thrust split), payload reductions offer only limited fuel savings. In the second retrofit study, both the conventional and electrified freighters carried the same payload. Due to the weight penalty associated with electrifying the propulsion system, the conventional aircraft had a lower TOGW than the electrified one. To save fuel with this operational strategy, the battery technology must mature to at least 1.0 kWh/kg. For 20% and 30% thrust splits, there exists a critical battery specific energy (at about 1.25 and 1.40 kWh/kg, respectively) in which a fuel savings is attained. Further increasing the battery specific energy beyond this point allows payload to be added back into the aircraft, thus improving its operational viability.

Future improvements to FAST will help improve its analytical robustness and usability. Enhancing the GPMs within FAST to refine historical regressions will boost predictive accuracy across key performance metrics. Secondly, unifying the governing equations for the climb, cruise, and descent segments could simplify the mission analysis, streamlining both code maintenance and aircraft performance evaluation. Additionally, incorporating analytical differentiation may

[¶]https://dx.doi.org/10.7302/26047

enable gradient-based optimization, making FAST more adaptable for sensitivity analyses and broader optimization tasks critical to early-phase aircraft design.

X. Appendix

Appendix X.A provides simple examples of input files for FAST. Appendix X.B is a follow-up to the energy-based segment analysis from Section V.A and provides an algorithm for the reader to replicate the analysis. Appendix X.C is a follow-up to the off-design gas turbine engine modeling from Section VI.C and provides the necessary coefficients to estimate the fuel flow to power a turbofan engine. Section X.D describes the mission profiles used to validate the Airbus A320Neo and Embraer E175LR from Section VII.

A. Example Input Files

Figures 15 and 16 illustrate examples of an Aircraft Specification File and Mission Profile Specification File, respectively. All figures generated from MATLAB codes were formatted for publication using `mcode` [50].

```
%% TOP-LEVEL AIRCRAFT REQUIREMENTS %%
%%%%%%%%%%%%%%%%%%%%%%%%%%%%%%%%%%%%

% entry to service year
Aircraft.Specs.TLAR.EIS = 2016;

% aircraft class
Aircraft.Specs.TLAR.Class = "Turbofan";

% approximate number of maximum passengers
Aircraft.Specs.TLAR.MaxPax = 150;


%% VEHICLE PERFORMANCE %%
%%%%%%%%%%%%%%%%%%%%%%%%

% design range (m)
Aircraft.Specs.Performance.Range = ...
    UnitConversionPkg.ConvLength(2150,'naut mi','m');

%% PROPULSION %%
%%%%%%%%%%%%%%%%

% propulsion architecture
Aircraft.Specs.Propulsion.Arch.Type = 'C';
```

Fig. 15 Example aircraft specification.

```
%% DEFINE THE MISSION TARGETS %%
%%%%%%%%%%%%%%%%%%%%%%%%%%%%%%%%

% define the targets (in m or min)
Mission.Target.Valu = [3981800;  45];

% define the target types ("Dist" or "Time")
Mission.Target.Type = ["Dist";  "Time"];


%% DEFINE THE MISSION SEGMENTS %%
%%%%%%%%%%%%%%%%%%%%%%%%%%%%%%%%

% define the segments
Mission.Segs = ["Takeoff"; "Climb"; "Cruise"; "Descent"; "Landing"];

% define the mission id (segments in same mission must be consecutive)
Mission.ID   = [        1;       1;        1;         1;         1];

% define the starting/ending altitudes (in m)
Mission.AltBeg = [      0;       0;    10668;     10668;      1524];
Mission.AltEnd = [      0;   10668;    10668;      1524;         0];

% define the climb rate (in m/s)
Mission.ClbRate = [   NaN;     NaN;      NaN;       NaN;       NaN];

% define the starting/ending speeds (in m/s or mach)
Mission.VelBeg  = [     0;    72.0;     0.78;      0.78;     102.9];
Mission.VelEnd  = [  72.0;    0.78;     0.78;     102.9;         0];

% define the speed types (either "TAS", "EAS", or "Mach")
Mission.TypeBeg = [ "TAS";   "TAS";   "Mach";    "Mach";     "TAS"];
Mission.TypeEnd = [ "TAS";  "Mach";   "Mach";     "TAS";     "TAS"];
```

Fig. 16 Excerpt from a mission profile specification.

B. Energy-Based Segment Analysis Algorithm

The algorithm used to perform the energy-based segment analysis in Section V.A is provided in Algorithm 1.

Algorithm 1 Energy-based mission analysis.

Discretize the segment into n points
Input $h^{(1)}$, $V_\infty^{(1)}$, $h^{(n)}$, and $V_\infty^{(n)}$
Initialize altitudes at control points by linearly interpolating between $h^{(1)}$ and $h^{(n)}$
Initialize airspeeds at control points by linearly interpolating between $V_\infty^{(1)}$ and $V_\infty^{(n)}$
Compute the energy heights using $H_e = h + \frac{(V_\infty)^2}{2g}$
if aircraft is a turbofan **then**
    Compute the thrust power using $\mathcal{T}V_{\infty,\text{turbofan}} = \left(\mathcal{T}_{\text{SLS}}\frac{\rho}{\rho_{\text{SLS}}}\right)V_\infty$
else
    Compute the thrust power using $\mathcal{T}V_{\infty,\text{turboprop/piston}} = P_{\text{SLS}}\left(\frac{\rho}{\rho_{\text{SLS}}}\right)^m$
end if
Predict the lift using $L = mg\cos(\alpha)$
Predict the drag using $D = \frac{L}{(L/D)}$
Compute the specific excess power using $P_s = \frac{\mathcal{T}V_\infty - DV_\infty}{W}$
if rate of climb is provided **then**
    Compute the time to climb using $\Delta t = \frac{\Delta h}{(dh/dt)}$
    Compute the maximum realizable acceleration using $\left(\frac{dV}{dt}\right)_{\text{max}} = \frac{(P_s - dh/dt)g}{V_\infty}$
    if any $\frac{dV_\infty}{dt} > \left(\frac{dV_\infty}{dt}\right)_{\text{max}}$ **then**
        Set $\frac{dV_\infty}{dt} = \left(\frac{dV_\infty}{dt}\right)_{\text{max}}$ where applicable
        Re-compute the airspeed profile: $V_\infty^{(i)} = V_\infty^{(i-1)} + \left(\frac{dV_\infty}{dt}\right)^{(i-1)}\Delta t^{(i-1)}$
    end if
else
    Compute Δt using $\Delta t = \left|\frac{\Delta H_e}{P_s}\right|$
    if any $\frac{dh}{dt} > \left(\frac{dh}{dt}\right)_{\text{max}}$ **then**
        Set $\frac{dh}{dt} = \left(\frac{dh}{dt}\right)_{\text{max}}$ where applicable
        Re-compute the time to climb using $\Delta t = \frac{\Delta h}{(dh/dt)}$
    end if
end if
Compute the rate of climb using $\frac{dh}{dt} = \frac{\Delta h}{\Delta t}$
Compute the acceleration using $\frac{dV_\infty}{dt} = \frac{\Delta V_\infty}{\Delta t}$
Compute the aircraft-level power required using $P_{\text{req}} = DV_\infty + W\frac{dh}{dt} + \frac{1}{2}mV_\infty\frac{dV_\infty}{dt}$
Propagate the aircraft-level power required to the components in the propulsion system
Compute the energy required by each energy source using $E_{\text{req, ES}} = \sum_{i=1}^{n-1}\left(P_{\text{req, ES}}\right)^{(i)}\Delta t^{(i)}$

C. Off-design turbofan engine modeling coefficients

In Section VI.C, Eqs. 19 through 21 explained how to compute the fuel flow in a turbofan engine using data from the *ICAO Aircraft Emissions Databank* [30]. Table 12 lists the required coefficients to estimate the fuel flow for a variety of turbofan engines.

Table 12 Off-design turbofan engine modeling coefficients and cruise TSFC.

Engine	$C_{ff,3}\left(\frac{\text{kg}}{\text{s}}\right)$	$C_{ff,2}\left(\frac{\text{kg}}{\text{s}}\right)$	$C_{ff,1},\left(\frac{\text{kg}}{\text{s}}\right)$	$C_{ff,ch}\left(\frac{\text{kg}}{\text{kN}\times\text{s}\times\text{m}}\right)$	$\text{TSFC}_{\text{cr}}\left(\frac{\text{kg}}{\text{kN}\times\text{s}\times\text{m}}\right)$
CF34-8E5	0.2992	−0.3464	0.7012	7.8175×10^{-7}	1.93×10^{-2}
LEAP1A26	0.3940	−0.4938	0.9638	6.8249×10^{-7}	1.44×10^{-2}
LEAP1B25	0.4033	−0.4374	0.9833	6.6083×10^{-7}	1.50×10^{-2}
Trent 772	1.5189	−1.5650	3.2532	5.5180×10^{-7}	1.60×10^{-2}
CFM56-7B20	0.4248	−0.6031	1.0944	7.4318×10^{-7}	1.79×10^{-2}
CFM56-7B24	0.4708	−0.5909	1.2262	7.0206×10^{-7}	1.78×10^{-2}
CFM56-5C4	0.3928	−0.3230	1.3895	5.4289×10^{-7}	1.54×10^{-2}
CFM56-5C3	0.3720	−0.3372	1.3415	5.5485×10^{-7}	1.54×10^{-2}
CFM56-5C2	0.4172	−0.4225	1.3165	5.6145×10^{-7}	1.54×10^{-2}
CFM56-5B4	0.4107	−0.4658	1.2238	5.1770×10^{-7}	1.54×10^{-2}
CFM56-5B2	0.5168	−0.4719	1.3839	4.7575×10^{-7}	1.54×10^{-2}
CFM56-5B1	0.4273	−0.3966	1.3314	6.2608×10^{-7}	1.69×10^{-2}
CFM56-5A1	0.4370	−0.5006	1.1176	6.9397×10^{-7}	1.69×10^{-2}
CFM56-3B2	0.5239	−0.7323	1.2685	7.6016×10^{-7}	1.89×10^{-2}
CFM56-3B1	0.4970	−0.7408	1.1938	7.7482×10^{-7}	1.89×10^{-2}
TFE731-2-2B	0.1099	−0.1797	0.2755	8.1211×10^{-7}	2.31×10^{-2}
TFE731-3	0.1594	−0.2396	0.3059	7.8088×10^{-7}	2.32×10^{-2}
CF6-6D	0.6881	−0.8084	1.8619	7.8130×10^{-7}	1.83×10^{-2}
CF6-50A	0.6427	−0.7307	2.2570	7.9211×10^{-7}	1.85×10^{-2}
CF6-50C	0.5913	−0.5759	2.2664	7.9039×10^{-7}	1.86×10^{-2}
CF6-50E	0.5826	−0.5468	2.3256	7.8372×10^{-7}	1.86×10^{-2}
CF6-80A	0.1966	−0.1296	2.0786	6.9091×10^{-7}	1.76×10^{-2}
CF6-80C2A1	0.8280	−0.7522	2.3288	6.5360×10^{-7}	1.63×10^{-2}
GE90-85B	1.3008	−1.3348	3.2336	6.2196×10^{-7}	1.47×10^{-2}
JT8D-7	0.7009	−0.9494	1.2431	7.1991×10^{-7}	2.25×10^{-2}
JT8D-9	0.7856	−1.0425	1.3023	7.0552×10^{-7}	2.27×10^{-2}
JT8D-17	1.0575	−1.3668	1.5596	5.5773×10^{-7}	2.27×10^{-2}
JT9D-7	0.4007	−0.5522	2.2412	6.7839×10^{-7}	1.76×10^{-2}
JT9D-20	0.2833	−0.4244	2.2468	6.8476×10^{-7}	1.77×10^{-2}
PW2037	0.3800	−0.2765	1.4395	7.8166×10^{-7}	1.65×10^{-2}
RB211-22B	1.4623	−2.0834	2.5004	7.0212×10^{-7}	1.78×10^{-2}
Tay 611-8C	0.6785	−1.0341	1.1006	6.1175×10^{-7}	2.01×10^{-2}

D. Mission Profiles and Calibration Factors for Validation

In Section VII, FAST was validated by sizing notional Airbus A320Neo and Embraer ERJ175LR models. Tables 13 and 14 define the mission profiles used to size the notional A320Neo and ERJ175LR, respectively. Table 15 lists the factors used while calibrating the notional models.

Table 13 Notional A320Neo design mission profile.

Mission	Segment	Initial Altitude (ft)	Final Altitude (ft)	Initial Airspeed (kts or Mach)	Final Airspeed (kts or Mach)
First Cruise – 1,133 nmi	Takeoff	0	0	0 KTAS	Mach 0.30
	Initial Climb	0	10,000	Mach 0.30	250 KTAS
	Main Climb	10,000	35,000	250 KTAS	Mach 0.78
	Cruise	35,000	35,000	Mach 0.78	Mach 0.78
Second Cruise – 1,133 nmi	Climb	35,000	37,000	Mach 0.78	Mach 0.78
	Cruise	37,000	37,000	Mach 0.78	Mach 0.78
Third Cruise – 1,133 nmi	Climb	37,000	39,000	Mach 0.78	Mach 0.78
	Cruise	39,000	39,000	Mach 0.78	Mach 0.78
	Descent	39,000	1,500	Mach 0.78	Mach 0.30
Divert – 200 nmi	Climb	1,500	15,000	Mach 0.30	Mach 0.30
	Cruise	15,000	15,000	Mach 0.30	Mach 0.30
	Descent	15,000	1,500	Mach 0.30	Mach 0.30
Loiter – 30 minutes	Cruise	1,500	1,500	Mach 0.30	Mach 0.30
	Descent	1,500	0	Mach 0.30	Mach 0.30
	Landing	0	0	Mach 0.30	0 KTAS

Table 14 Notional ERJ175LR design mission profile.

Mission	Segment	Initial Altitude (ft)	Final Altitude (ft)	Initial Airspeed (kts or Mach)	Final Airspeed (kts or Mach)
Design Mission – 2,150 nmi	Takeoff	0	0	0 KTAS	135 KTAS
	Initial Climb	0	3,000	135 KTAS	200 KEAS
	Main Climb	3,000	35,000	200 KEAS	200 KEAS
	Accelerate	35,000	35,000	200 KEAS	Mach 0.78
	Cruise	35,000	35,000	Mach 0.78	Mach 0.78
	Decelerate	35,000	35,000	Mach 0.78	210 KEAS
	Main Descent	35,000	3,000	210 KEAS	210 KEAS
	Final Descent	3,000	1,500	210 KEAS	162 KTAS
Divert – 100 nmi	Initial Climb	1,500	3,000	162 KTAS	200 KEAS
	Main Climb	3,000	9,000	200 KEAS	200 KEAS
	Final Climb	9,000	10,000	200 KEAS	250 KTAS
	Divert	10,000	10,000	250 KTAS	250 KTAS
Loiter – 45 min	Loiter	10,000	10,000	250 KTAS	250 KTAS
	Initial Descent	10,000	9,000	250 KTAS	200 KEAS
	Main Descent	9,000	3,000	200 KEAS	200 KEAS
	Final Descent	3,000	0	200 KEAS	162 KTAS
	Landing	0	0	162 KTAS	0 KTAS

Table 15 Calibration factors for notional aircraft models.

Calibration Factor	Notional A320Neo	Notional ERJ175LR
Airframe Weight Factor	0.993	1.018
Fuel Flow Factor	1.092	1.029
Climb Lift-to-Drag Ratio	1.000	1.002
Cruise Lift-to-Drag Ratio	1.000	1.000

Funding Sources

This work is sponsored by the NASA Aeronautics Research Mission Directorate and Electrified Powertrain Flight Demonstration project, "Development of a Parametrically Driven Electrified Aircraft Design and Optimization Tool", Glenn Engineering and Research Support Contract (GEARS) Contract No. 80GRC020D0003.

Acknowledgments

The authors would like to thank Ralph Jansen, Amy Chicatelli, Andrew Meade, Karin Bozak, Noah Listgarten, Dennis Rohn, and Gaudy Bezos-O'Connor from NASA's Electrified Powertrain Flight Demonstration project for supporting this work and providing valuable technical input and feedback throughout the duration of the project. The authors also thank Huseyin Acar, Rawan Aljaber, Swapnil Jagtap, Nawa Khailany, Janki Patel, Joaquin Rey, Jayda Shine, and Michael Tsai for their contributions to either FAST or the Aerobase that the regressions and projections rely on.

AI-based editing assistance was used (Grammarly and ChatGPT) for grammar and language refinement during manuscript preparation. The tool did not contribute to the research design, analysis, or interpretation of results.

References

[1] Jansen, R., Brown, G. V., Felder, J. L., and Duffy, K. P., "Turboelectric aircraft drive key performance parameters and functional requirements," *51st AIAA/SAE/ASEE joint propulsion conference*, 2015, p. 3890. https://doi.org/https://doi.org/10.2514/6.2015-3890.

[2] National Aeronautics, and Space Administration, "Electrified Aircraft Propulsion (EAP)," https://www1.grc.nasa.gov/aeronautics/eap/, 2024.

[3] National Aeronautics, and Space Administration, "About Electrified Powertrain Flight Demonstration Project," https://www.nasa.gov/directorates/armd/integrated-aviation-systems-program/armd-iasp-epfd/about-electrified-powertrain-flight-demonstration-project/, 2022.

[4] National Aeronautics and Space Administration, "Subsonic Single Aft Engine (SUSAN) Aircraft," https://www1.grc.nasa.gov/aeronautics/eap/airplane-concepts/susan/, 2023.

[5] National Aeronautics and Space Administration, "Single-Aisle Turboelectric Aircraft with Aft Boundary Layer Propulsion (STARC-ABL)," https://www1.grc.nasa.gov/aeronautics/eap/airplane-concepts/starc-abl/, 2023.

[6] Lukaczyk, T. W., Wendorff, A. D., Colonno, M., Economon, T. D., Alonso, J. J., Orra, T. H., and Ilario, C., "SUAVE: an open-source environment for multi-fidelity conceptual vehicle design," *16th AIAA/ISSMO Multidisciplinary Analysis and Optimization Conference*, 2015, p. 3087. https://doi.org/https://doi.org/10.2514/6.2015-3087.

[7] Kruger, M., "The Challenges and Potential Benefits of Electrified Propulsion for Aircraft," Ph.D. thesis, University of Southern California, 2022.

[8] Wu, E., Kenway, G., Mader, C. A., Jasa, J., and Martins, J. R., "pyOptSparse: A Python framework for large-scale constrained nonlinear optimization of sparse systems," *Journal of Open Source Software*, Vol. 5, No. 54, 2020, p. 2564. https://doi.org/https://doi.org/10.21105/joss.02564.

[9] Gratz, J., Kirk, J., Recine, C., Jasa, J., Aretskin-Hariton, E., Moore, K., and Marfatia, K., "Aviary: An Open-Source Multidisciplinary Design, Analysis, and Optimization Tool for Modeling Aircraft with Analytic Gradients," *AIAA AVIATION FORUM AND ASCEND 2024*, 2024, p. 4219. https://doi.org/https://doi.org/10.2514/6.2024-4219.

[10] Gray, J. S., Hwang, J. T., Martins, J. R. R. A., Moore, K. T., and Naylor, B. A., "OpenMDAO: An open-source framework for multidisciplinary design, analysis, and optimization," *Structural and Multidisciplinary Optimization*, Vol. 59, No. 4, 2019, pp. 1075–1104. https://doi.org/https://doi.org/10.1007/s00158-019-02211-z.

[11] David, C., Delbecq, S., Defoort, S., Schmollgruber, P., Benard, E., and Pommier-Budinger, V., "From FAST to FAST-OAD: An open source framework for rapid Overall Aircraft Design," *IOP Conference Series: Materials Science and Engineering*, Vol. 1024, IOP Publishing, 2021, p. 012062. https://doi.org/https://doi.org/10.1088/1757-899X/1024/1/012062.

[12] De Vries, R., Hoogreef, M. F., and Vos, R., "Range equation for hybrid-electric aircraft with constant power split," *Journal of Aircraft*, Vol. 57, No. 3, 2020, pp. 552–557. https://doi.org/https://doi.org/10.2514/1.C035734.

[13] Harish, A., Gladin, J., and Mavris, D., "Universal Range Equation for Unconventional Aircraft Concepts," *2022 IEEE Transportation Electrification Conference & Expo (ITEC)*, IEEE, 2022, pp. 1057–1063. https://doi.org/https://doi.org/10.1109/ITEC53557.2022.9814012.

[14] Trifari, V., Ruocco, M., Cusati, V., Nicolosi, F., and De Marco, A., "Multi-disciplinary analysis and optimization Java tool for aircraft design," *Proceedings of the 31st ICAS Conference (International Council of the Aeronautical Sciences), Belo Horizonte, Brazil*, 2018, pp. 9–14. https://doi.org/https://doi.org/10.2514/6.2022-3737.

[15] Nicolosi, F., De Marco, A., Attanasio, L., and Vecchia, P. D., "Development of a Java-based framework for aircraft preliminary design and optimization," *Journal of Aerospace Information Systems*, Vol. 13, No. 6, 2016, pp. 234–242. https://doi.org/https://doi.org/10.2514/1.I010404.

[16] Trifari, V., De Marco, A., Di Stasio, M., Ruocco, M., Nicolosi, F., Grazioso, G., Ahuja, V., and Hartfield, R., "An aircraft design workflow using the automatic knowledge-based modelling tool JPAD Modeller," *AIAA AVIATION 2022 Forum*, 2022, p. 3737. https://doi.org/https://doi.org/10.2514/6.2022-3737.

[17] Martins, J. R. R. A., and Ning, A., *Engineering Design Optimization*, Cambridge University Press, 2021.

[18] Cinar, G., "A methodology for dynamic sizing of electric power generation and distribution architectures," Ph.D. thesis, Georgia Institute of Technology, 2018.

[19] Cinar, G., Cai, Y., Chakraborty, I., and Mavris, D. N., "Sizing and optimization of novel general aviation vehicles and propulsion system architectures," *2018 Aviation Technology, Integration, and Operations Conference*, 2018, p. 3974. https://doi.org/https://doi.org/10.2514/6.2018-3974.

[20] Cinar, G., Cai, Y., Bendarkar, M. V., Burrell, A. I., Denney, R. K., and Mavris, D. N., "System analysis and design space exploration of regional aircraft with electrified powertrains," *Journal of Aircraft*, Vol. 60, No. 2, 2023, pp. 382–409. https://doi.org/https://doi.org/10.2514/1.C036919.

[21] IDEAS Laboratory, "FAST Aerobase," , 2024. URL https://github.com/ideas-um/FAST/tree/main/%2BDatabasePkg.

[22] Arnson, M., Aljaber, R., and Cinar, G., "Predicting Aircraft Design Parameters using Gaussian Process Regressions on Historical Data," *AIAA SciTech 2025 Forum*, 2025, p. 1287. https://doi.org/https://doi.org/10.2514/6.2025-1287.

[23] Khailany, N., Mokotoff, P. R., and Cinar, G., "Aircraft Geometry and Propulsion Architecture Visualization for the Future Aircraft Sizing Tool (FAST)," *AIAA SciTech Forum*, 2025, p. 1288. https://doi.org/https://doi.org/10.2514/6.2025-1288.

[24] Cinar, G., Garcia, E., and Mavris, D. N., "A framework for electrified propulsion architecture and operation analysis," *Aircraft Engineering and Aerospace Technology*, Vol. 92, No. 5, 2020, pp. 675–684. https://doi.org/https://doi.org/10.1108/AEAT-06-2019-0118.

[25] Wang, Y.-C., Stockhausen, M., Mokotoff, P. R., and Cinar, G., "SUbsonic Single Aft eNgine (SUSAN) System Integration Analysis with the Future Aircraft Sizing Tool (FAST)," *AIAA SciTech 2025 Forum*, 2025, p. 2376. https://doi.org/https://doi.org/10.2514/6.2025-2376.

[26] Schlickenmaier, H. W., Anderson, M., Harrison, E., Hooper, E. H., Knickerbocker, J., Larson, M., Lawson, J., Voss, M., WIlkinson, R., and Turnberg, J., "X-57 Maxwell Airworthiness Validation Plan," Tech. rep., HS Advanced Concepts, LLC, 2023.

[27] Ascher, U. M., and Greif, C., *A first course on numerical methods*, SIAM, 2011.

[28] Duffy, K. P., and Jansen, R. H., "Turboelectric and hybrid electric aircraft drive key performance parameters," *2018 AIAA/IEEE Electric Aircraft Technologies Symposium (EATS)*, IEEE, 2018, pp. 1–19. https://doi.org/https://doi.org/10.2514/6.2018-5023.

[29] Tremblay, O., and Dessaint, L.-A., "Experimental Validation of a Battery Dynamic Model for EV Applications," *World Electric Vehicle Journal*, Vol. 3, No. 2, 2009, pp. 289–298. https://doi.org/10.3390/wevj3020289.

[30] European Union Aviation Safety Agency, "ICAO Aircraft Engine Emissions Databank," https://www.easa.europa.eu/en/domains/environment/icao-aircraft-engine-emissions-databank, 2024.

[31] Roux, E., *Turboshaft, Turboprop & Propfan Database Handbook*, Editions Elodie Roux, 2011.

[32] Roux, E., *Turboshaft, Turboprop and Propfan: Database Handbook*, Éditions Élodie Roux, 2011.

[33] Mattingly, J. D., Heiser, W. H., Boyer, K. M., Haven, B. A., and Pratt, D. T., *Aircraft Engine Design, Third Edition*, American Institute of Aeronautics and Astronautics, Inc., 2018. https://doi.org/10.2514/4.105173.

[34] Boyce, M. P., *Gas Turbine Engineering Handbook*, 2nd ed., Butterworth-Heinemann, Oxford, England, 2001.

[35] Walsh, P. P., and Fletcher, P., *Gas Turbine Performance*, 2nd ed., Blackwell Science, Philadelphia, PA, 2004.

[36] Saravanamuttoo, H., Rogers, G. F. C., and Cohen, H., *Gas Turbine Theory*, 5th ed., Prentice Hall, Philadelphia, PA, 2001.

[37] Anderson, J. D., *Aircraft performance and design*, WCB/McGraw-Hill, Boston, Mass., 1999.

[38] Sun, J., Hoekstra, J. M., and Ellerbroek, J., "OpenAP: An Open-Source Aircraft Performance Model for Air Transportation Studies and Simulations," *Aerospace*, Vol. 7, No. 8, 2020. https://doi.org/10.3390/aerospace7080104.

[39] Meier, N., "Civil Turbojet/Turbofan Specifications," https://jet-engine.net/civtfspec.htm, 2021.

[40] Karnozov, V., "Aviadvigatel Mulls Higher-thrust PD-14s To Replace PS-90A," https://www.ainonline.com/aviation-news/air-transport/2019-08-19/aviadvigatel-mulls-higher-thrust-pd-14s-replace-ps-90a, 2019.

[41] EMBRAER S.A., "Airport planning manual," https://www.embraercommercialaviation.com/wp-content/uploads/2017/02/APM_E175.pdf, 2005.

[42] AIRBUS, "A320neo," https://aircraft.airbus.com/en/aircraft/a320-the-most-successful-aircraft-family-ever/a320neo, 2024.

[43] FSAirlines, "A320neo Specification," https://remote.fsairlines.net/v1/acdetails.php?ac=168100&rvi=19945, 2010.

[44] AIRBUS, "A320 Aircarft characteristics airport and maintenance planning," https://www.airbus.com/sites/g/files/jlcbta136/files/2021-11/Airbus-Commercial-Aircraft-AC-A320.pdf, 2005.

[45] Federal Aviation Administration, "FAA Type Certificate Data Sheet No. A56NM," , 2022. URL https://drs.faa.gov/browse/excelExternalWindow/22037ED8FF40F56A862587D4004E3443.0001.

[46] Lockheed Martin Aeronautics Company, "LM-100J," https://www.lockheedmartin.com/content/dam/lockheed-martin/aero/documents/LM-100J/LM-100JBrochure_F2018_Website.pdf, 2018.

[47] Pham, D., Bowles, J. V., Zilliac, G. G., Listgarten, N., Go, S., and Jansen, R. H., "Parametric Modeling and Mission Performance Analysis of a True Parallel Hybrid Turboprop Aircraft for Freighter Operations," *AIAA AVIATION FORUM AND ASCEND 2024*, 2024, p. 3581. https://doi.org/https://doi.org/10.2514/6.2024-3581.

[48] Pham, D. D.-T. V., Recine, C., and Jansen, R. H., "Sizing and Performance Analysis of a MW-Class Electrified Aircraft Propulsion (EAP) System for a Parallel Hybrid Turboprop Concept," *34th Congress of the International Council of the Aeronautical Sciences (ICAS)*, 2024.

[49] Federal Aviation Administration, "Type Certificate Data Sheet No. A1SO," https://drs.faa.gov/browse/excelExternalWindow/6B8971BD3E1EBB4F862584C5006C541A.0001?modalOpened=true, 2019.

[50] Korn, F., "`mcode.sty` Demo," https://www.overleaf.com/latex/templates/highlighting-matlab-code-in-latex-with-mcode/nhtksndnsmmx.pdf, 2014.